Dear Editor,

Thank you very much for the opportunity to improve our manuscript. We agree with your comment about the conclusion section and have rewritten it following your advice. We also added a reference on our paper in GMDD (Sec. 4.2), where we in detail described WRF-Chem code modifications.

Alexander Ukhov
Georgiy Stenchikov

Assessment of natural and anthropogenic aerosol air pollution in the Middle East using MERRA-2, CAMS data assimilation products, and high-resolution WRF-Chem model simulations

Alexander Ukhov[1], Suleiman Mostamandi[1], Arlindo da Silva[2], Johannes Flemming[3], Yasser Alshehri[1], Illia Shevchenko[1], and Georgiy Stenchikov[1]

[1]King Abdullah University of Science and Technology, Thuwal, Saudi Arabia
[2]NASA Goddard Space Flight Center, Greenbelt, MD, USA
[3]European Centre for Medium-Range Weather Forecasts, Reading, UK

Correspondence: Georgiy Stenchikov (georgiy.stenchikov@kaust.edu.sa)

Abstract. Modern-Era Retrospective analysis for Research and Applications v.2 (MERRA-2), Copernicus Atmosphere Monitoring Service Operational Analysis (CAMS-OA), and a high-resolution regional Weather Research and Forecasting model coupled with Chemistry (WRF-Chem) were used to evaluate natural and anthropogenic Particulate Matter (PM) air pollution in the Middle East (ME) during 2015-2016. Two Moderate Resolution Imaging Spectrometer (MODIS) retrievals: combined product Deep Blue and Deep Target (MODIS-DB&DT), Multi-Angle Implementation of Atmospheric Correction (MAIAC), and Aerosol Robotic Network (AERONET) aerosol optical depth (AOD) observations, as well as *in situ* PM measurements for 2016, were used for validation of the WRF-Chem output and both assimilation products.

MERRA-2 and CAMS-OA assimilate AOD observations. WRF-Chem is a free-running model, but dust emission in WRF-Chem is tuned to fit AOD and aerosol volume size distributions obtained from AERONET. MERRA-2 was used to construct WRF-Chem initial and boundary conditions both for meteorology and chemical/aerosol species. SO_2 emissions in WRF-Chem are based on the novel OMI-HTAP SO_2 emission dataset.

The correlation with the AERONET AOD is highest for MERRA-2 (0.72-0.91), MAIAC (0.63-0.96), and CAMS-OA (0.65-0.87), followed by MODIS-DB&DT (0.56-0.84) and WRF-Chem (0.43-0.85). However, CAMS-OA has a relatively high positive mean bias with respect to AERONET AOD. The spatial distributions of seasonally averaged AODs from WRF-Chem, assimilation products, and MAIAC are well correlated with MODIS DB&DT AOD product. MAIAC has the highest correlation (R=0.8) followed by MERRA-2 (R=0.66), CAMS-OA (R=0.65), and WRF-Chem (R=0.61). WRF-Chem, MERRA-2, and MAIAC underestimate, and CAMS-OA overestimates MODIS-DB&DT AOD.

The simulated and observed PM concentrations might differ of a factor of two, because of it is more challenging to the model and the assimilation products to reproduce PM concentration measured within the city. Although aerosol fields in WRF-Chem and assimilation products are entirely consistent, WRF-Chem, due to its higher spatial resolution and better SO_2 emissions, is preferable for analysis of regional air-quality over the ME. The WRF-Chem's PM background concentrations exceed the World Health Organization (WHO) guidelines over the entire ME. Mineral dust makes the major contributor to PM ($\approx$75–95%) compared to other aerosol types. Near and down the wind from the SO_2 emission sources, non-dust aerosols (primarily sulfate)

contribute up to 30% into PM2.5. The contribution of sea salt into PM in coastal regions can reach 5%. The contributions of organic matter, black and organic carbon into PM over the Middle East are insignificant. In the major cities over the Arabian peninsula, the 90th percentile of PM_{10} and $PM_{2.5}$ daily mean surface concentrations exceed the corresponding Kingdom Saudi Arabia air-quality limits. The contribution of the non-dust component to $PM_{2.5}$ is < 25%, which limits the emission control effect on air quality. The mitigation of the dust effect on air quality requires the development of environment-based approaches like growing tree belts around the cities and enhancing in-city vegetation cover. The presented in this study WRF-Chem configuration could be a prototype of a future air quality forecast system that warn the population against air pollution hazards.

1 Introduction

PM is a complex mixture of sea salt, sulfate, black carbon, organic matter, and mineral dust, suspended in the air. The dramatic increase in the level of air pollution in developing countries over the last decades is forced by rapid economic and population growth, burning of fossil fuels, construction, and agricultural activities (Janssens-Maenhout et al., 2015). However, the primary cause of air pollution in the ME is mineral dust, and it is on the rise (Klingmüller et al., 2016). Along with Asia and Africa, the ME significantly contributes to global dust emissions, which are in the range of 1000-2000 $\mathrm{Tg/year}$ (Zender et al., 2004). According to Prospero et al. (2002), the Middle East and North Africa (MENA) regions account for about half of global dust emissions. By integrating surface emissions in MERRA-2 reanalysis we found that, the total global dust emission averaged over the 2015-2016 period is about 1600 $\mathrm{Tg/year}$, right in the middle of the Zender et al. (2004) estimate. The dust emission from our simulation domain (see Fig. 1) that covers the ME and nearby areas is about 500 $\mathrm{Tg/year}$, contributing ≈30% to the global dust emission budget. Also, frequent inflows of pollutants from Europe, Africa, and India, worsen the air quality over the Arabian Peninsula (Jish Prakash et al., 2015; Kalenderski et al., 2013; Notaro et al., 2013; Reid et al., 2008; Mohalfi et al., 1998; Kalenderski and Stenchikov, 2016; Parajuli et al., 2019). Because of the large amount of dust, the ME is one of the most polluted areas in the world. Located in the center of the northern subtropical dust belt, the Arabian Desert is the third-largest (after the Sahara and the East Asian deserts) region of dust generation, where dust plays a significant role in controlling regional climate (Cahill et al., 2017; Banks et al., 2017; Jish Prakash et al., 2016; Farahat, 2016; Kalenderski and Stenchikov, 2016; Munir et al., 2013; Alghamdi et al., 2015; Lihavainen et al., 2016; Anisimov et al., 2017; Osipov and Stenchikov, 2018).

In addition to natural dust aerosols, the ME receives high concentrations of anthropogenic PM (Karagulian et al., 2015; Al-Taani et al., 2019; Alharbi et al., 2015; Khodeir et al., 2012). The most important anthropogenic aerosol in ME is sulfate with SO_2 as a precursor, the contributions of other types of aerosols in PM, sea salt, organic matter, and black carbon are of lesser importance in the ME (Randles et al., 2017). ME emits about 10% of the total global anthropogenic SO_2 (Klimont et al., 2013). SO_2 produced in the course of power generation, water desalination, and oil recovery operations (Al-Jahdali and Bisher, 2008) is converted photochemically into sulfate aerosol, which contributes to PM and has significant adverse effects on human health (Lelieveld et al., 2015). Ukhov et al. (2020b) simulated SO_2 transport and distribution over the Middle east using the high-resolution WRF-Chem model and demonstrated high surface concentrations of SO_2 along the west and east coasts of Arabian Peninsula.

The impact of aerosols on air-quality is characterized by near-surface concentrations of PM, which comprise both PM_{10} and $PM_{2.5}$ (particles with diameters less than 10 μm and 2.5 μm, correspondingly). Extended exposure to PM may cause cardiovascular and respiratory disease, lung cancer, and cause premature mortality on a global scale (Lelieveld et al., 2015). According to the WHO, outdoor air pollution caused 4.2 million premature deaths worldwide in 2016 (WHO, 2018). To protect human health and the environment WHO (WHO, 2006), and the National Agencies, e.g., the United States Environmental Protection Agency (US-EPA) (USEPA, 2010), European Commission (EC) (EUEA, 2008), and Kingdom Saudi Arabia Presidency of Meteorology and Environment (KSA-PME) (PME, 2012) issued the air quality regulations for PM that are presented in Table 1. The WHO regulations are the strictest, while KSA-PME regulations are the softest.

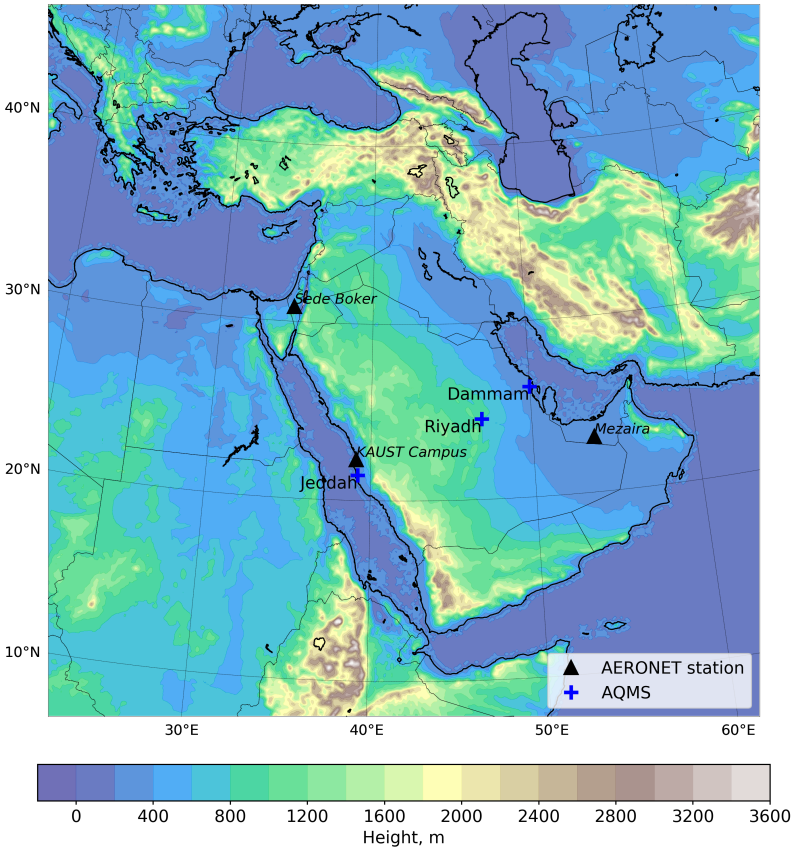

Figure 1. Simulation domain with marked locations of the AQMS and AERONET sites.

Global satellite observations of aerosol optical depth (AOD) inform about vertically-integrated aerosol loading in an entire atmospheric column. But the near-surface PM concentration can not be observed from the space. These measurements could be conducted only *in situ* in a limited number of locations. Along with instrumental observations, modern data assimilation products provide valuable information about AOD and near-surface PM concentration even in areas where satellite sensors are unreliable due to factors such as the high reflectivity of land surfaces (Shi et al., 2011). Assimilation products improve

Table 1. Air quality regulations for $PM_{2.5}$ and PM_{10} prescribed by WHO, US-EPA, EC, and KSA-PME, $\mu g/m^3$.

	Aver. period	WHO	US-EPA	EC	KSA-PME
$PM_{2.5}$	24 hours	25	35[1]	-	35
	1 year	10	15[2]	25	15
PM_{10}	24 hours	50	150[4]	50[3]	340
	1 year	20	-	40	80

[1] 98th percentile, averaged over 3 years

[2] annual mean, averaged over 3 years

[3] 35 permitted exceedances per year

[4] not to be exceeded more than once per year on average over 3 years

the aerosol total column loadings through the assimilation of observed AOD but are not capable of assimilating the aerosol vertical structure and chemical composition. There are two well known data assimilation products that assimilate atmospheric constituents: MERRA-2 (Randles et al., 2017; Buchard et al., 2017) from National Aeronautics and Space Administration (NASA) Goddard Space Flight Center (GSFC) and CAMS-OA (Inness et al., 2019; Flemming et al., 2015; Inness et al., 2015) from European Centre for Medium-range Weather Forecast (ECMWF). These data assimilation products adequately reproduce AOD and PM concentrations at different regions of the world (Provençal et al., 2017; Buchard et al., 2017; Cesnulyte et al., 2014; Cuevas et al., 2014). E.g., Provençal et al. (2017) tested PM surface concentrations from the MERRA Aerosol Reanalysis (predecessor of MERRA-2) against observations over Europe. Buchard et al. (2017) evaluated MERRA-2 surface $PM_{2.5}$ on the global scale and over the continental United States. Excessive validation of the Monitoring Atmospheric Composition and Climate (MACC) reanalysis (predecessor of CAMS) has been conducted by Cesnulyte et al. (2014), who compared the model AOD with the AERONET observations. Cuevas et al. (2014) evaluated atmospheric mineral dust from the MACC reanalysis has been evaluated over the MENA region for 2007–2008 using satellite and ground-based observations. MERRA-2 and CAMS-OA are global and have a relatively low spatial resolution (in comparison with the regional models), which diminishes their ability to resolve fine-scale regional spatial features. Like any other model, MERRA-2 and CAMS-OA use emission inventories of anthropogenic pollutants that may be outdated and incomplete, especially in the rapidly developing parts of the world, like the ME region (McLinden et al., 2016). E.g., SO_2 emissions used in MERRA-2 and CAMS-OA differ by 45-50% in some ME regions (Ukhov et al., 2020b).

In this study, we evaluate aerosol outputs from MERRA-2, CAMS-OA, and WRF-Chem over the ME, against satellite, ground-based AOD observations, and *in situ* $PM_{2.5}$ and PM_{10} measurements during 2015-2016 period, and assess air pollution over the ME focusing on the following science questions:

1. How accurately do WRF-Chem, MERRA-2, and CAMS-OA capture the abundance of dust aerosol, its volume size, and spatial distributions over the ME, in comparison with AERONET and satellite observations?

2. How accurately do WRF-Chem, MERRA-2, and CAMS-OA capture PM surface concentrations compared with *in situ* measurements?

3. What are the contributions of dust, sea salt, sulfate, black carbon, and organic matter in PM surface concentrations?

4. What is the overall impact of PM pollution on air quality over the ME region and in the ME major cities?

The paper is organized as follows: Section 2 describes the observational datasets used in this study. Section 3 characterizes data assimilation products. In Section 4, the WRF-Chem model setup is described. In Section 5, the capabilities of WRF-Chem, MERRA-2, and CAMS-OA to simulate dust aerosol abundance over the ME are compared; the PM spatial distributions and PM air pollution in the ME major cities obtained from the WRF-Chem simulations are also discussed. Conclusions are presented in Section 6.

2 Observational datasets

To evaluate the data assimilation products and WRF-Chem output, we use Moderate Resolution Imaging Spectrometer (MODIS) AOD retrievals, ground-based Aerosol Robotic Network (AERONET) AOD observations, and aerosol volume size distribution retrievals, as well as *in situ* measurements of PM surface concentrations.

2.1 AERONET

AERONET comprises more than 1000 observation sites equipped with CIMEL sunphotometers and PREDE skyradiometers manufactured in France by CIMEL and in Japan by PREDE. They measure direct sun and sky radiances at eight wavelengths (340, 380, 440, 500, 670, 870, 940, and 1020 nm) every 15 minutes during daylight time (Holben et al., 1998). In 2012 we established the *KAUST Campus* site, which is currently the only permanently operational AERONET site in Saudi Arabia. For this study we have chosen three AERONET sites (*KAUST Campus*, *Mezaira*, and *Sede Boker*, see Fig. 1) that routinely collected data in 2015-2016 and are located within our domain. We utilized level 2.0 (cloud screened and quality assured) AERONET AOD data. To facilitate comparison with the model output the 550 nm AOD is calculated using the following relation:

$$\frac{\tau_\lambda}{\tau_{\lambda_0}} = \left(\frac{\lambda}{\lambda_0}\right)^{-\alpha} \tag{1}$$

where α is the Ångström exponent for the 440-675 nm wavelength range provided by AERONET, τ_λ is the optical thickness at wavelength λ, and τ_{λ_0} is the optical thickness at the reference wavelength λ_0. From here forward, we presume that AOD is given or calculated at 550 nm.

In addition to direct observations of AOD, the AERONET retrieval algorithm provides column integrated Aerosol Volume Size Distribution (AVSD) *dV*/*d*lnr ($\mu\mathrm{m}^3/\mu\mathrm{m}^2$) on 22 logarithmically equidistant discrete points in the range of radii between 0.05 and 15 $\mu\mathrm{m}$ (Dubovik and King, 2000). We use these retrievals to evaluate the AVSDs calculated by WRF-Chem, CAMS-OA, and MERRA-2.

2.2 MODIS

MODIS instruments on-board the NASA TERRA and AQUA satellites provide aerosol properties over both land and ocean with near-daily global coverage. The standard MODIS AOD aerosol product combines two retrieval algorithms: 1) the MODIS dark-target (DT) algorithm (Kaufman et al., 1997) is used over the ocean and dark areas with sufficient vegetation, 2) the Deep Blue (DB) algorithm is used over bright desert surfaces of the Sahara and the ME. From this combined product (MODIS-DB&DT v6.1) we use AOD at 550 nm level 2 data from the daily dataset at 10 km spatial resolution, downloaded from https://ladsweb.modaps.eosdis.nasa.gov/about/purpose (Levy et al., 2015).

Recently, a new MODIS AOD product became available that was obtained using the Multi-Angle Implementation of Atmospheric Correction (MAIAC) algorithm (Lyapustin et al., 2018). This algorithm uses time series analysis and image processing to derive the surface bidirectional reflectance function at fine spatial resolution. MAIAC uses empirically tuned, spatially varying, aerosol properties derived from the AERONET climatology, and provides AOD at 470 and 550 nm with 1 km spatial resolution over land globally. We include the new MAIAC product (version 6, level 2) in the comparison between simulated and retrieved AODs.

2.3 Surface *in situ* PM observations

To test the model-produced PM concentrations, we use observations conducted by the air quality monitoring stations (AQMS) that measure surface concentrations of $PM_{2.5}$ and PM_{10} in Riyadh, Jeddah, and Dammam (megacities of Saudi Arabia), see Fig. 1. Observations are available starting from 2016. The measurements were conducted by the Saudi Authority for Industrial Cities and Technology Zones (MODON). MODON uses MP101M analyzer to continuously detect $PM_{2.5}$ and PM_{10} concentrations by measuring the absorption of low-energy β-radiation that is proportional to the mass of aerosol particles independently of their physicochemical nature (measurement Method ISO 10473). $PM_{2.5}$ and PM_{10} measurement error is $\pm$ 5%. The system satisfies the European Standards EN 12341 and US EPA (40CFR part 53) for PM_{10} and EN 14907 for $PM_{2.5}$ continuous monitoring. The PM measurements are conducted every 15 minutes, and collected data are transmitted in real-time to servers at MODON for processing and storage. To provide confidence in the operational status of the each AQMS, a comprehensive physical audit is conducted quarterly by Ricardo-AEA Ltd, (https://www.ctc-n.org/network/network-members/ricardo-aea-ltd).

3 Data assimilation products

MERRA-2 and CAMS-OA assimilate satellite observations to provide aerosol abundance and air-quality data globally. MERRA-2 also assimilates AERONET AODs. In contrast, WRF-Chem is a free-running model and does not assimilate observations.

3.1 MERRA-2

MERRA-2 (https://gmao.gsfc.nasa.gov/reanalysis/MERRA-2) provides meteorological and atmospheric composition fields on $0.625^\circ \times 0.5^\circ$ latitude-longitude grid and 72 terrain-following hybrid $\sigma - p$ model layers (Randles et al., 2017; Buchard et al.,

2017). The pressure at the model top equals 0.01 hPa. MERRA-2 uses the Goddard Earth Observing System, version 5 (GEOS-5) atmospheric model (Rienecker et al., 2008), which is interactively coupled to the Goddard Global Ozone Chemistry Aerosol Radiation and Transport (GOCART) model (Chin et al., 2002, 2014) (i.e., it takes into account the effects of aerosols on radiation and model dynamics). This model simulates dust and sea salt in five size bins (see Tab. 2), $\mathrm{SO_2}$, sulfate, organic and black carbon (hydrophobic and hydrophilic), $\mathrm{O_3}$, CO, dimethyl sulfide (DMS), and methane sulfonic acid (MSA). The dust density is 2600 $\mathrm{kg/m^3}$ for all sizes. Dust and sea salt emissions are calculated in the model, depending on the near-surface wind. The dust source function is taken from Ginoux et al. (2001). For anthropogenic emissions, MERRA-2 employs the EDGAR-4.2 (Janssens-Maenhout et al., 2013) emission inventory available on a $0.1^\circ \times 0.1^\circ$ grid. MERRA-2 assimilated AOD at 550 nm from the Advanced Very High-Resolution Radiometer (AVHRR) (Heidinger et al., 2014) over the oceans until 2002. Since 2000 MERRA-2 started assimilating MODIS and Multiangle Imaging SpectroRadiometer (MISR) (Kahn et al., 2005) data over land and ocean. Both instruments are on the TERRA satellite which has an equatorial overpass at 10:30 am UTC, while AVHRR has mostly orbited with the afternoon equatorial crossing time. Therefore MERRA-2 continued using AVHRR data over the ocean until 2002 when the AQUA satellite was launched. Since AQUA has an orbit with the equator overpass at 2:30 pm UTC, AVHRR data was no longer needed for coverage. We have to mention that MERRA-2 assimilates specially processed MODIS observations, not the standard MODIS-DB&DT aerosol product. It also assimilates AERONET AODs (Randles et al., 2017).

3.2 CAMS-OA

CAMS-OA (https://atmosphere.copernicus.eu/) has been conducted in almost real-time since July 2012. The CAMS-OA product has a resolution of $0.8^\circ \times 0.8^\circ$ before 21 June 2016, and $0.4^\circ \times 0.4^\circ$ after that, with 60 vertical levels. It employs the ECMWF aerosol data assimilation system developed within the Integrated Forecast System (IFS) (Morcrette et al., 2009; Benedetti et al., 2009). The extended version of the Carbon Bond chemical mechanism 5 (CB05) (Yarwood et al., 2005) is implemented in the IFS (Flemming et al., 2015). CB05 describes tropospheric chemistry with 54 species and 126 reactions. The chemistry scheme is coupled with the aerosol module.

CAMS-OA simulates five aerosol species: dust, sea salt, sulfate, organic carbon, and black carbon. To calculate dust and sea salt, it uses three dust-bins (see Tab. 2). The dust density is 2600 $\mathrm{kg/m^3}$ for all bins. Emissions of mineral dust and sea salt depend on simulated near-surface wind speed. Dust emission is parameterized following Marticorena and Bergametti (1995) with the source function adopted from Ginoux et al. (2001). $\mathrm{SO_2}$ oxidation into sulfate aerosol is parameterized using a prescribed latitude-dependent e-folding timescale ranging from 3 days at the equator to 8 days at the poles. The anthropogenic emissions for the chemical species are taken from the MACCity inventory (Granier et al., 2011), which is available on a $0.5^\circ \times 0.5^\circ$ grid and covers the period 1960–2010. CAMS-OA assimilates MODIS AQUA and TERRA AODs. It uses observations from Collection 5 since 2009, and Deep Blue since 2015.

Table 2. Radii ranges (μm) of dust and sea salt bins used in GOCART model (WRF-Chem, MERRA-2) and in CAMS-OA.

	Bin				
	1	2	3	4	5
CAMS-OA dust	0.03-0.55	0.55-0.9	0.9-20.0	-	-
CAMS-OA sea salt	0.03-0.5	0.5-5.0	5.0-20.0	-	-
GOCART dust	0.1-1.0	1.0-1.8	1.8-3.0	3.0-6.0	6.0-10.0
GOCART sea salt	0.03-0.1	0.1-0.5	0.5-1.5	1.5-5.0	5.0-10.0

4 WRF-Chem

To calculate fine-resolution PM and sulfate fields, we use the Weather Research and Forecasting (WRF) model (Skamarock et al., 2005) coupled with chemistry (WRF-Chem v3.7.1) (Grell et al., 2005). The WRF-Chem is used for prediction and simulation of weather, air quality, and dust storms, accounting for the aerosol effect on radiation. WRF-Chem can be configured with one of the few gas-phase chemical mechanisms, photolysis, and aerosols parameterization models. WRF-Chem has been widely used for air quality simulations in different parts of the globe: East Asia (Wang et al., 2010), North America (Kim et al., 2006; Chuang et al., 2011), Europe (Forkel et al., 2012; Ritter et al., 2013), South America (Archer-Nicholls et al., 2015) and Middle East (Parajuli et al., 2019). To reduce the clock-time of our two-year calculations, we simulated each month of the 2015-2016 period separately. Each simulation starts from the last week of the previous month. This time is considered a spin-up and is excluded from post-processing. The simulation domain, shown in Fig. 1, is centered at 28°N, 42°E, and a 10×10 km^2 horizontal grid (450×450 grid nodes) is employed. The vertical grid comprises 50 vertical levels with enhanced resolution closer to the ground comprising 11 model levels within the near-surface 1-km layer. The model top boundary is set at 50 hPa.

To improve the representation of the meteorological fields, we apply spectral nudging (Miguez-Macho et al., 2004) above the planetary boundary layer (PBL) ($>$5.0 km) to horizontal wind components (U and V) toward the MERRA-2 wind field. The nudging coefficient for U and V is set to be 0.0001 s^{-1}. We only nudge waves with wavelengths longer than 450 km. This allows us to keep the large-scale motions close to reanalysis, and leave the resolved small-scale, high-frequency features unaffected.

The aerosol/chemistry initial and boundary conditions (IC&BC) are calculated using MERRA-2 output using the newly developed *Merra2BC* interpolation utility (Ukhov and Stenchikov, 2020). To be consistent with aerosol/chemistry IC&BC, we also define the meteorological IC&BC using MERRA-2 output (see Appendix A1).

The following set of physical parameterizations was used in WRF-Chem runs. The Unified Noah land surface model (*sf_surface_physics*=2) and the Revised MM5 Monin-Obukhov scheme (*sf_sfclay_physics*=1) are chosen to represent land surface processes and surface layer physics. The Yonsei University scheme is chosen for PBL parameterization (*bl_pbl_physics*=1). The WRF single moment microphysics scheme (*mp_physics*=4) is used for the treatment of cloud microphysics. The New Grell scheme (*cu_physics*=5) is used for cumulus parameterization. The Rapid Radiative Transfer Model (RRTMG) for both

short-wave (*ra_sw_physics*=4) and long-wave (*ra_lw_physics*=4) radiation is used for radiative transfer calculations. Only the aerosol direct radiative effect is accounted for. More details on the physical parameterizations used can be found at http://www2.mmm.ucar.edu/wrf/users/phys_references.html.

4.1 Gas-phase chemistry and aerosols

To calculate the atmospheric chemistry within WRF-Chem, we employ the Regional Atmospheric Chemistry Mechanism (RACM, *chem_opt*=301) (Stockwell et al., 1997) containing 77 species and 237 reactions, which include 23 photolysis reactions, but no heterogeneous chemistry. The RACM chemical module is embedded into WRF-Chem using the Kinetic PreProcessor (KPP) (Damian et al., 2002). The role of KPP is to integrate the system of stiff nonlinear ordinary differential equations, which represents the specified set of chemical reactions. The photolysis rates are calculated on-line according to Madronich (1987) (*phot_opt*=1). Similar to MERRA-2, the GOCART chemistry module is used to calculate $\mathrm{SO_2}$ to sulfate oxidation (Chin et al., 2002, 2014) by the hydroxyl radical OH whose abundance is interactively simulated by RACM.

We use the novel OMI-HTAP $\mathrm{SO_2}$ emission dataset (Liu et al., 2018) based on the combination of distributed $\mathrm{SO_2}$ emissions from residential and transportation sectors, taken from the HTAP-2.2 inventory (Janssens-Maenhout et al., 2015) with the catalogue of the strong ($>30\ \mathrm{kt/year}$) $\mathrm{SO_2}$ point emissions (Fioletov et al., 2016) built using satellite observations by Ozone Monitoring Instrument (OMI) (Levelt et al., 2006; Li et al., 2013). The catalogue contains more than 500 point sources of industrial origin, some of which are not present in the widely used EDGAR-4.2 and HTAP-2.2 emission datasets. For example, 14 previously unaccounted $\mathrm{SO_2}$ point emissions located in the ME (mostly in the Arabian Gulf) were detected, most of them are related to oil and gas industry. OMI-HTAP divides $\mathrm{SO_2}$ emissions into surface and elevated ones. We distribute the surface $\mathrm{SO_2}$ emissions with a constant mixing ratio in the 0-1000 m layer, and elevated emissions in 120-1000 m layer. All other constituents (other PM from biogenic and fossil components, black and organic carbon, etc.), including $\mathrm{SO_2}$ shipping emissions, are taken from the HTAP-2.2 inventory and are treated as surface emissions. OMI-HTAP $\mathrm{SO_2}$ emissions are provided on $0.1^\circ \times 0.1^\circ$ grid (Liu et al., 2018). We conservatively interpolated them on the WRF-Chem $10 \times 10\ \mathrm{km^2}$ grid. See Ukhov et al. (2020b) for details.

To calculate aerosols we employ the GOCART (Chin et al., 2002) aerosol model (*chem_opt=301*). It is the same microphysical model as that used in MERRA-2 (see Sec. 3.1). Dust and sea salt size distributions in WRF-Chem are approximated by the same five dust and sea-salt size bins as those in MERRA-2 (Tab. 2). However, only the last four "salt" bins in Tab. 2 are used in WRF-Chem, as the first bin appears to be very poorly populated. Dust density is assumed to be 2500 $\mathrm{kg/m^3}$ for the first dust-bin and 2650 $\mathrm{kg/m^3}$ for 2-5 dust-bins. Emission of sea salt is calculated according to Gong (2003). Dust emission from the surface is calculated using the GOCART emission scheme (Ginoux et al., 2001) (*dust_opt=1*). Dust emission mass flux, F_p (μg $\mathrm{m^{-2}\ s^{-1}}$) in each dust-bin p=1,2,...,5 is defined by the relation:

$$F_p = \begin{cases} CSs_p u_{10m}^2 (u_{10m} - u_t), & \text{if } u_{10m} > u_t \\ 0, & \text{otherwise} \end{cases} \tag{2}$$

where, C has the dimension of ($\mu g\ s^2\ m^{-5}$) and is a spatially uniform factor which controls the magnitude of dust emission flux; S is the spatially varying topographic source function (Ginoux et al., 2001) that characterizes the spatial distribution of dust emissions; u_{10m} is the horizontal wind speed at 10 m height; u_t is the threshold velocity, which depends on particle size and surface wetness; s_p is a fraction of dust mass emitted into dust-bin p, $\sum s_p = 1$.

To avoid natural dust emission in urban areas, we use the built-in WRF-Chem the U.S. Geological Survey (USGS) 24-category land-use data set (Anderson, 1976). We modify the source function S using the following expression:

$$S' = (1.0 - URBAN\_MASK) \cdot S \tag{3}$$

where S' is the modified topographic source function, $URBAN\_MASK$ is the USGS "*Urban and Built-up Land*" mask field. It has the sense of a fraction of urban area in a grid-cell and ranges from 0 to 1. Grid cells with $URBAN\_MASK$=1 do not produce natural dust emissions. We do not account for anthropogenic dust emissions within cities, and therefore potentially underestimate urban dust pollution.

As in our previous studies (Kalenderski et al., 2013; Jish Prakash et al., 2015; Anisimov et al., 2017), we tune dust emissions to fit the AOD from the AERONET stations located within the domain. For this purpose, the factor C from Eq. (2) has been adjusted to achieve the best agreement between simulated and observed AOD at *KAUST Campus, Mezaira*, and *Sede Boker* AERONET sites, see Fig. 1. Assuming that factor C does not depend on time and geographical coordinates, we can only tune the annual average AOD bias. Both simulations and observations represent the total AOD with contributions from all types of aerosols. Because dust dominates all other aerosols in the ME, we choose to tune only the dust emissions. Obtained during test runs, C value of 0.5 is kept constant in all subsequent production runs. We also tune s_p from Eq. (2) to better reproduce the AVSDs provided by AERONET inversion algorithm. This tuning and the comparisons of AOD and AVSDs from the assimilation products and WRF-Chem simulations are discussed in detail below.

In situ air quality observations in the Middle east are scarce. It is one of the known problems for air quality research in this area. The things are simplified a bit by the fact that in the ME dust dominates aerosol pollution. E.g., Cloud-Aerosol Lidar and Infrared Pathfinder Satellite Observations (CALIPSO) (Vaughan et al., 2004) records dust in 95% of profiles (Osipov et al., 2015). The effect of nitrates, ammonia, and organics on AOD and PMs is insignificant; therefore, the employed aerosol-chemical scheme (GOCART-RACM) is adequate for the ME conditions. To support this conclusion, we have conducted laboratory analysis of the chemical composition of soil and dust deposition samples that show a little presence of organics and ammonium (Jish Prakash et al., 2016; Engelbrecht et al., 2017). According to Engelbrecht et al. (2017), in 2015, the annual average weight percentages of soluble ions of ammonium (NH_4) and sulfate in deposition samples taken at four sites at the *KAUST Campus* are 0.05% and 2.513%, respectively. It means that available ammonium may neutralize at a maximum of 5% of sulfate mass. The actual contribution of ammonium sulfate should be lower, as some ammonium may also be bound as ammonium nitrate, ammonium phosphate, or ammonium chloride.

4.2 WRF-Chem code modification

We have corrected the source code of the WRF-Chem v3.7.1 with GOCART aerosol module in several places. These corrections were implemented in the WRF-Chem v4.1.3 official release. We evaluate how they change the results in ~~the forthcoming technical publication~~Ukhov et al. (2020a). Here we only briefly discuss the introduced changes and their effects. Firstly, the diagnostic output of PM concentrations was corrected, because contributions of the individual dust and sea salt bins were incorrectly calculated. Therefore, $PM_{2.5}$ surface concentrations were erroneously underestimated by 7% while PM_{10} - were overestimated by 5%. Secondly, we found that the contribution of fine dust particles with radii $<$0.46 μm was omitted in the calculation of AOD, AOD was consequently underestimated by 25-30%. This led to an overestimation of the dust emission flux because we force the simulated AOD to match the AERONET observations. Thirdly, we fixed the dust and sea salt gravitational settling subroutine, since initially, the calculations of mass fluxes of settling particles did not account for changes in air density. Due to this error, the total mass of dust and sea salt aerosols increased, violating mass conservation.

5 Results

5.1 Regional climate and circulation

The ME is one of the hottest and driest regions on the Earth. Summer in the ME is long and hot with little precipitation. Precipitation mainly occurs in the south-west of the Arabian Peninsula. Winter is mild, with rainfall being mostly associated with cold fronts and cyclones propagating from the Eastern Mediterranean (Climate.com, 2018). Emission and transport of dust are driven by winds. Emission and deposition of dust are also sensitive to soil moisture and precipitation (Furman, 2003; Shao, 2008; Yu et al., 2015). However, because the ME is an arid region, the soil moisture and precipitation effects are insignificant.

Figure 2 shows contours of sea level pressure, topographic source function S (Ginoux et al., 2001), and seasonally 2015-2016 averaged wind speed barbs at 10 m height over the ME during winter (DJF) and summer (JJA) from WRF-Chem simulations. Over northeast Africa in winter (see Fig. 2a), the strong pressure gradient between the Red Sea trough and the stationary high-pressure system over Egypt predominantly generates moderate north-easterly winds (up to 10 m/s). Therefore in winter, dust storms occur more frequently in the west of the Arabian Peninsula. Over the Central and Eastern Arabian Peninsula and the eastern part of the ME, winds are relatively weak and do not have a clear direction. However, cold fronts generated by Mediterranean cyclones can cause dust storms and dust transport to central regions of the Arabian Peninsula.

In summer (see Fig. 2b) the high-pressure system over the eastern Mediterranean and low-pressure system over the Arabian Gulf promote moderate north-northwesterly winds known as *Shamal* (Yu et al., 2016; Hamidi et al., 2013), which dominate over the central part of the Arabian peninsula. *Shamal* is the primary driver of dust storm events over this area (Yu et al., 2016; Shao, 2001; Middleton, 1986; Goudie and Middleton, 2006; Notaro et al., 2015). *Shamal* brings dust to the Arabian Gulf, north, and central part of Saudi Arabia, from the Tigris-Euphrates basin of Syria and Iraq (Anisimov et al., 2018).

Figure 3 shows wind speed seasonally averaged for 2015-2016 at 10 m from MERRA-2, CAMS-OA, and WRF-Chem during winter (DJF) and summer (JJA). WRF-Chem spatial distributions of wind speed agree well with MERRA-2 and CAMS-OA,

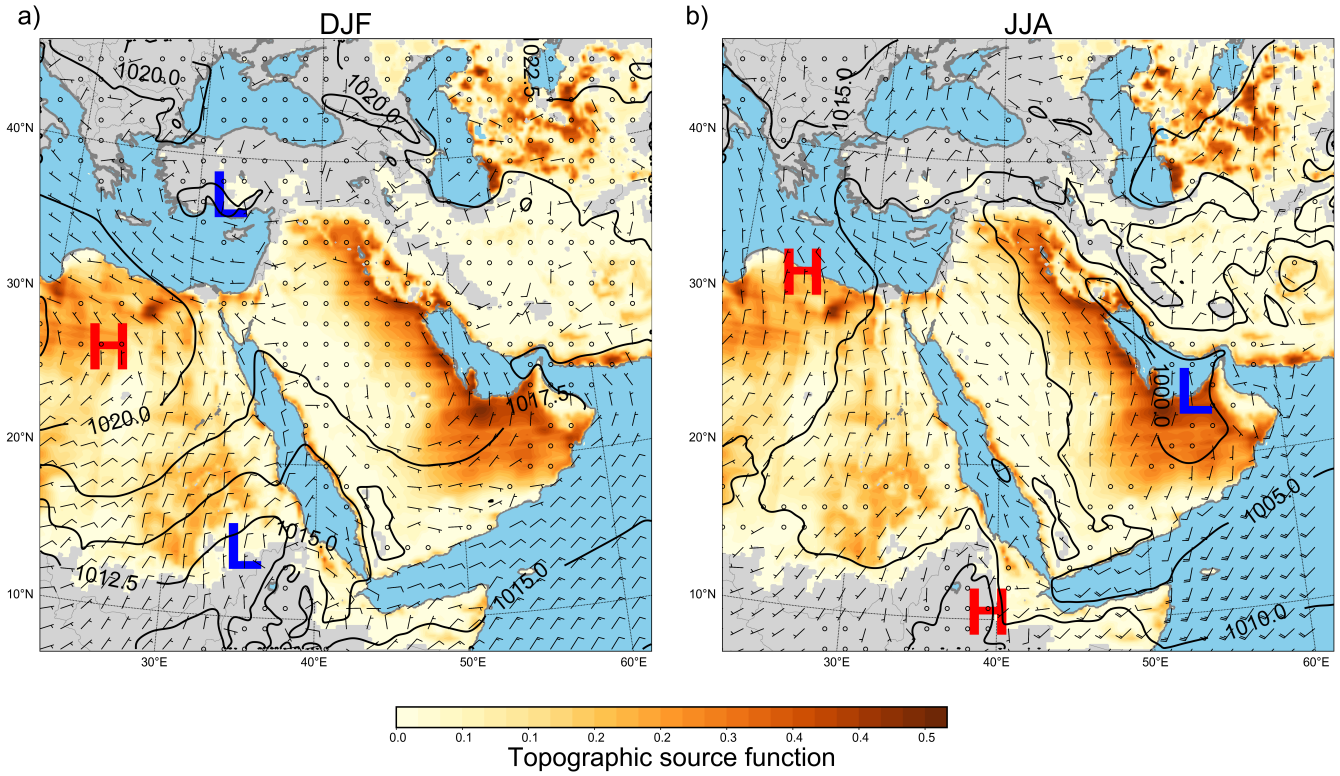

Figure 2. Seasonally averaged for 2015-2016 wind barbs ($\mathrm{m/s}$) at 10 m, sea level pressure (contours), and erodibility function (shading) (Ginoux et al., 2001). a) Winter (DJF), b) Summer (JJA).

but due to the higher spatial resolution, WRF-Chem better resolves the fine-scale spatial structures of the 10 m-wind field over complex terrain. All panels have similar seasonal variations of wind speed. In winter, maximum winds are stronger over the south-east of the domain. In the Central and northern parts of the domain winds are weak. In summer, wind speed increases in the northern and central parts of the ME. *Somali Jet* produces strong (10-15 $\mathrm{m/s}$) winds in the Arabian Sea along the coasts of Somalia and Oman.

To conduct the statistical analysis, we interpolated the seasonally averaged 2015-2016 zonal and meridional wind components (U and V) at 10 m from WRF-Chem, and CAMS-OA on MERRA-2 grid and calculated Pearson correlation coefficient (R), and root mean square differences ($RMSD$) between each pair, see Tab. 3, correspondingly. $RMSD$ is calculated using the same formula as the root mean square error ($RMSE$). The procedure of calculation of these parameters is given in Appendix A2. Pearson correlation coefficients provided in Tab. 3 are close to 1. The highest correlation is achieved between MERRA-2 and CAMS-OA. WRF-Chem's correlation coefficient with respect to MERRA-2 is smaller but exceeds that of the WRF-Chem - CAMS-OA pair. The WRF-Chem and MERRA-2 wind fields are close partly because WRF-Chem boundary conditions are built using MERRA-2 reanalysis, and the large-scale winds are nudged (see Sec. 4) to the ones from MERRA-2 over the PBL.

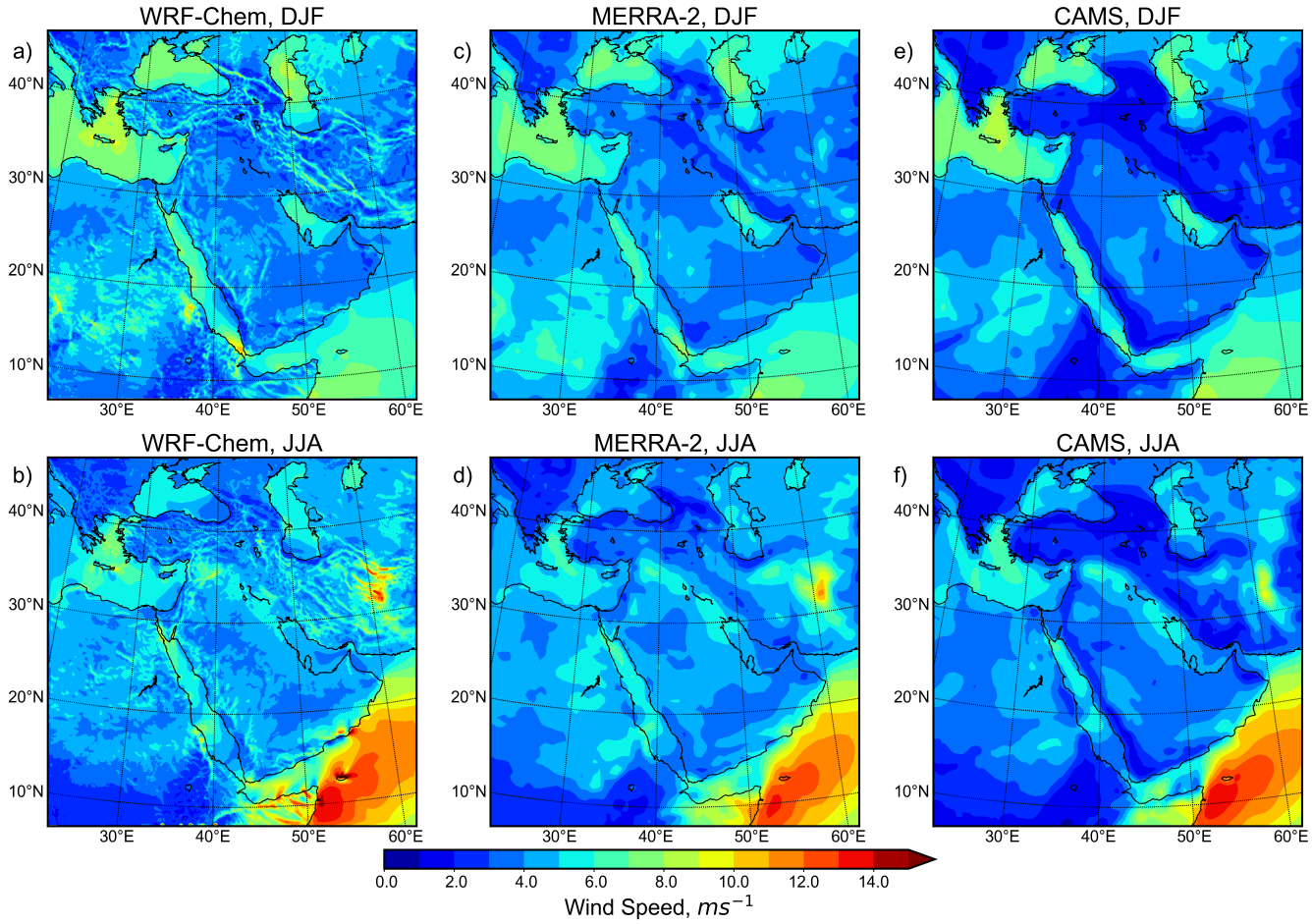

Figure 3. Seasonally averaged 2015-2016 wind speed at 10 m from WRF-Chem, MERRA-2, and CAMS-OA during winter (DJF), summer (JJA).

The $RMSDs$ (see Tab. 3) are lower in winter than in summer. All $RMSDs$ are in the range of 0.45-0.85 $\mathrm{m/s}$. The lowest $RMSDs$ are between MERRA-2 and CAMS-OA. Notably, the correlation coefficients for the meridional component V are higher, and the $RMSDs$ are lower when compared with the zonal wind component U. This is because the northern winds are stable since they are maintained by the large-scale processes. In contrast, the zonal wind component, which is affected by small-scale processes like sea-breezes, is variable. The results of the statistical analysis in Tab. 3 and the clear similarity of the spatial patterns (among all products) of the averaged 10 m wind fields presented in Fig. 3, suggest that WRF-Chem captures the magnitude and spatial distribution of the 10 m wind. Thus, we conclude that WRF-Chem with the selected set of physical parameterizations satisfactorily simulates both the large- and meso-scale atmospheric processes in the ME.

Table 3. Pearson correlation coefficient R and root mean square difference $RMSD$ $(\mathrm{m/s})$ for the seasonally averaged 2015-2016 wind components U and V at 10 m.

Season	WRF-Chem wrt CAMS-OA		WRF-Chem wrt MERRA-2		CAMS-OA wrt MERRA-2	
	R	$RMSD$	R	$RMSD$	R	$RMSD$
	$U \mid V$	$U \mid V$	$U \mid V$	$U \mid V$	$U \mid V$	$U \mid V$
Winter (DJF)	0.918 | 0.954	0.716 | 0.593	0.954 | 0.963	0.572 | 0.537	0.954 | 0.974	0.558 | 0.449
Summer (JJA)	0.929 | 0.981	0.853 | 0.704	0.938 | 0.982	0.833 | 0.669	0.965 | 0.986	0.636 | 0.593
Annual mean	0.924 | 0.968	0.785 | 0.649	0.946 | 0.973	0.703 | 0.603	0.960 | 0.980	0.597 | 0.521

* wrt - with respect to

5.2 AOD

In this section, we evaluate the ability of WRF-Chem, CAMS-OA, and MERRA-2 to reproduce the aerosol content in the atmosphere accurately. This content is characterized by AOD. In the ME, mineral dust contribution to the total AOD is dominant (≈87%) (Kalenderski and Stenchikov, 2016; Osipov et al., 2015). The treatment of optically active dust within the model is therefore vitally important. AOD is calculated based on aerosol concentrations and aerosol optical properties, which depend upon aerosol size distribution. We, therefore, evaluate how well WRF-Chem and assimilation products reproduce aerosol volume size distribution.

5.2.1 Aerosol volume size distributions

Dust particles are emitted into the lower atmospheric layer with some predominant size distribution (Martin and Kok, 2017; Kok, 2011). Emitted dust is processed by the atmosphere to produce the atmospheric dust size distribution that is retrieved by the AERONET inversion algorithm (Dubovik and King, 2000) and reported as column integrated AVSD. Strictly speaking, AERONET AVSD incorporates contributions from all types of aerosols. But the size distribution of emitted dust has the strongest effect on column integrated AVSD, because dust dominates all other aerosols in the ME. Therefore, we have to tune the dust emission parameters in the first place.

Eq. (2) assumes that emission mass fluxes into five dust size bins are controlled by the s_p fractions. In WRF-Chem the default values of s_p fractions for the five dust-bins (see Tab. 2) are {0.1, 0.25, 0.25, 0.25, 0.25}. We found that with these default s_p fractions, WRF-Chem underestimated the volume of fine dust particles in first bin 0.1 μm< r <1 μm compared with AERONET AVSD, whereas the volume of the second bin 1 μm< r <1.8 μm was overestimated. In combination with fitting the observed AOD by tuning of factor C, this led to an the increase of the total emitted dust mass, since fine particles are optically more efficient per unit mass than coarse particles. To achieve a better agreement between the simulated and AERONET AVSDs we adjusted fractions s_p to be {0.15, 0.1, 0.25, 0.4, 0.1}. A similar approach was implemented in Khan et al. (2015) using the MADE/SORGAM chemistry/aerosol scheme. This s_p modification is in line with (Adebiyi and Kok, 2020) as it effectively

decreased emission of dust particles with radii r<2.5 μm and increased emission of coarse particles with radii r>2.5 μm (see Appendix A3). We use the updated s_p values in all our WRF-Chem simulations.

Figure 4 shows seasonally averaged 2015-2016 volume size distributions obtained from MERRA-2, CAMS-OA, AERONET and WRF-Chem with updated s_p fractions. The comparison is conducted for the *KAUST Campus, Mezaira, Sede Boker* AERONET sites (see Fig. 1), since only these sites have information on AVSDs during the 2015-2016 period. The effect of s_p modification could be seen in Fig. 4 by comparing AVSDs from WRF-Chem with updated set of s_p and MERRA-2 that uses the default s_p set. A direct comparison of AVSDs from the WRF-Chem runs with the updated and default s_p sets is shown in Appendix A3.

Both MERRA-2 and WRF-Chem use the GOCART aerosol scheme with the same five dust-bins, and they approximate the shape of the AERONET AVSD relatively well. CAMS-OA uses only three dust-bins (see Tab. 2) and fails to reproduce the AERONET AVSD even qualitatively. It overestimates the volume of particles with radii of 0.55-0.9 μm and underestimates the volume of particles with radii of 0.9-20 μm. With the latest system upgrade in 2019, this weakness of CAMS-OA has been corrected by introducing of a new dust scheme (Nabat et al., 2012).

The volume size distributions from the model and assimilation products demonstrate pronounced seasonal variability with the increased amount of dust in the atmosphere during spring and summer. Since the *KAUST Campus* and *Mezaira* sites are located in the vicinity of the strong dust sources, the coarse mode at these sites is more pronounced than at the *Sede Boker* site, which is farther from the strong dust emission sources.

The fine mode in the AERONET AVSD is more pronounced at the *KAUST Campus* in comparison with the other AERONET sites due to its proximity to strong SO_2 sources located along the west coast of Saudi Arabia (Ukhov et al., 2020b). This proximity leads to a higher contribution of fine sulfate particles to the fine mode. The smaller volume of fine particles in the WRF-Chem and MERRA-2 simulated AVSD (see Fig. 4) is in part because the simulated AVSDs show only dust omitting the contributions of sulfate and sea salt. Sea salt particles/droplets are relatively large and mostly contribute to the coarse mode.

Figure 5 shows the contributions of dust, sea salt, and sulfate aerosols into the AVSD at the *KAUST Campus* AERONET site in WRF-Chem simulation averaged for two summer seasons (JJA) of 2015-2016. In WRF-Chem, sulfate aerosol is computed using a bulk approach. For calculating of aerosol optical properties, it is assumed that sulfate aerosol comprises two log-normal modes: nuclei and accumulation. According to WRF-Chem source code, the nuclei mode median radii μ_{nuc}=0.005 μm and geometric width σ_{nuc}=1.7, the accumulation mode median radii μ_{acc}=0.035 μm and geometric width σ_{acc}=2.0. The nuclei mode comprises 25% of the sulfate aerosol mass, and accumulation mode - 75%. It is assumed that sulfate aerosol density is 1800 $\mathrm{kg/m^3}$ and sea salt density is 2200 $\mathrm{kg/m^3}$. Figure 5 demonstrates that the contribution of the sulfate nuclei mode in the aerosol volume is almost negligible, while the sulfate accumulation mode adds in the volume of aerosol particles with radii <1 μm. The contribution of the sea salt aerosol into AVSD in WRF-Chem simulations is very little.

5.2.2 Comparison with AERONET AOD

The comparison of the daily averaged AOD time series and corresponding scatter plots calculated using WRF-Chem, MERRA-2, CAMS-OA, MODIS-DB&DT, and MAIAC data with AERONET AOD observations conducted at *KAUST Campus*, *Mezaira*

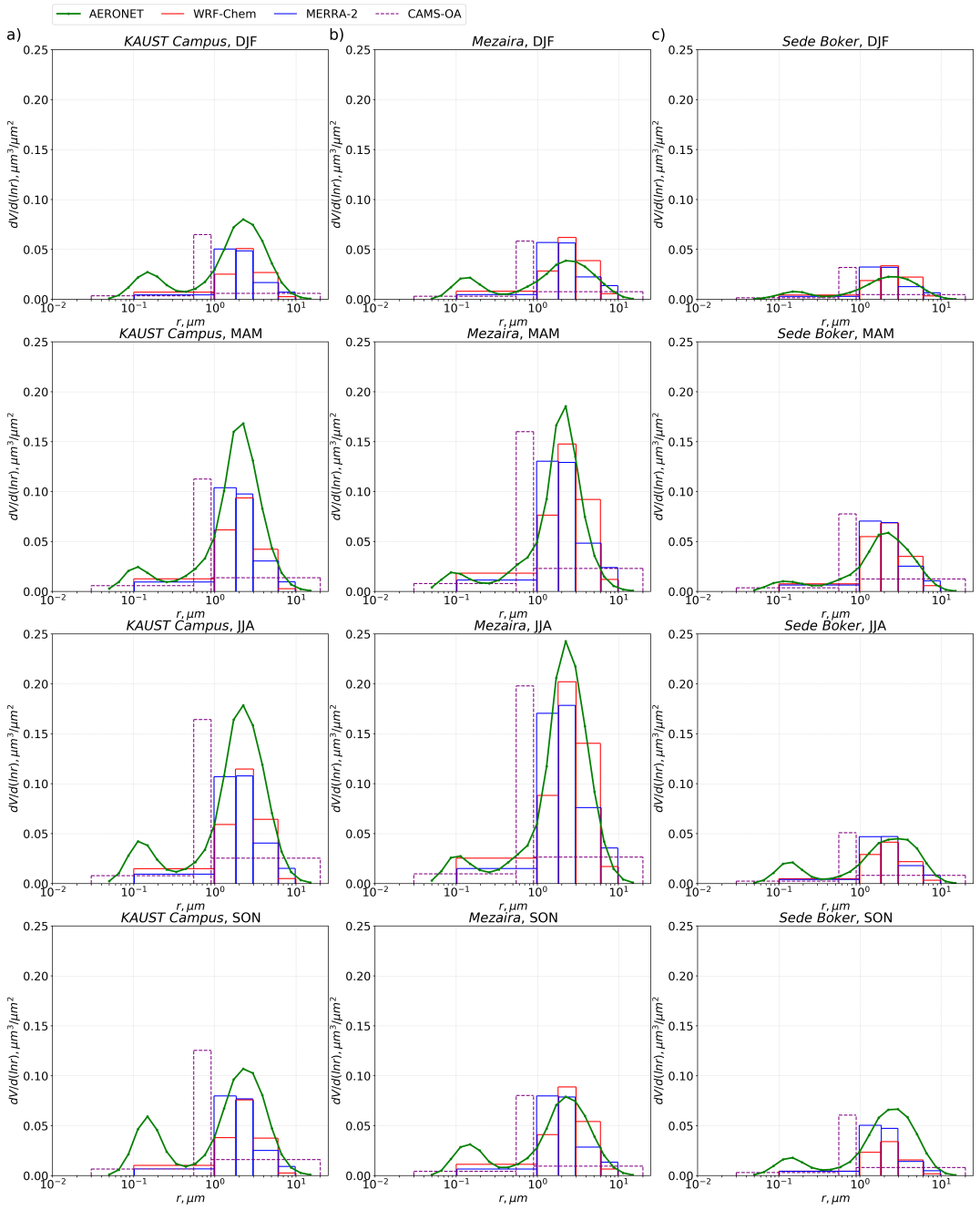

Figure 4. Seasonally averaged 2015-2016 AVSDs ($\mu m^3/\mu m^2$) obtained from MERRA-2, CAMS-OA, WRF-Chem, and from the AERONET inversion algorithm at a) *KAUST Campus*, b) *Mezaira* and c) *Sede Boker* AERONET sites. Winter (DJF), spring (MAM), summer (JJA) and autumn (SON).

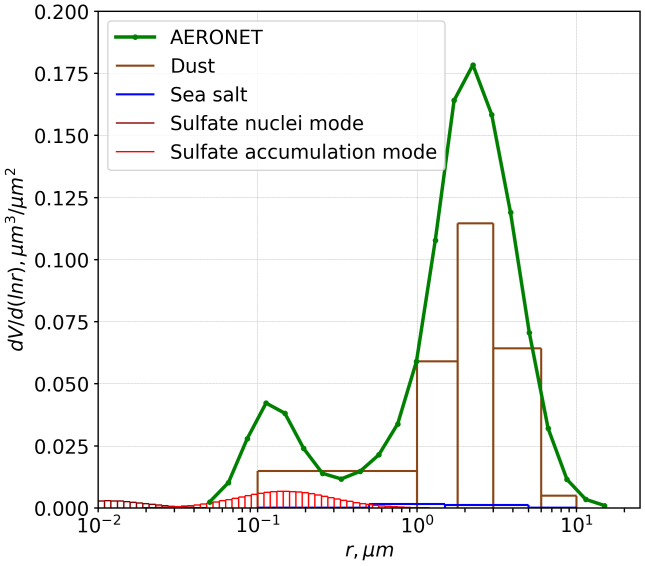

Figure 5. Summer (JJA) averaged 2015-2016 AVSD ($\mu m^3/\mu m^2$) at *KAUST Campus* AERONET site obtained from the AERONET inversion algorithm and from WRF-Chem.

Table 4. Pearson correlation coefficient *R* and mean bias calculated for daily averaged AOD time-series from WRF-Chem, CAMS-OA, MERRA-2, MODIS-DB&DT, and MAIAC with respect to AERONET AOD observations.

	WRF-Chem		CAMS-OA		MERRA-2		MODIS-DB&DT		MAIAC	
	bias	*R*	*bias*	*R*	*bias*	*R*	*bias*	*R*	*bias*	*R*
	2015									
KAUST Campus	-0.04	0.74	0.01	0.86	-0.05	0.85	0.06	0.81	-0.08	0.89
Mezaira	0.07	0.73	0.11	0.81	0.04	0.83	0.07	0.79	-0.07	0.88
Sede Boker	-0.01	0.43	0.07	0.65	0.02	0.72	0.06	0.84	0.04	0.96
	2016									
KAUST Campus	-0.01	0.75	0.01	0.76	-0.03	0.88	0.06	0.73	-0.05	0.74
Mezaira	0.09	0.62	0.12	0.87	0.06	0.85	0.08	0.77	-0.04	0.83
Sede Boker	0.03	0.85	0.09	0.83	0.04	0.91	0.08	0.56	0.05	0.63

380 and *Sede Boker* during 2015-2016 period is presented in Fig. 6. Because AERONET conducts observations only during the daylight time, we interpolated WRF-Chem, MERRA-2, CAMS-OA AODs to the AERONET measurements times and then conducted time averaging to make simulated and observed AODs consistent. AODs from MODIS-DB&DT and MAIAC are provided as a daily average. Although MODIS routinely provides observations only twice a day during daylight time, up to four observations might be collected on some days due to overlap of the TERRA and AQUA orbits at some locations.

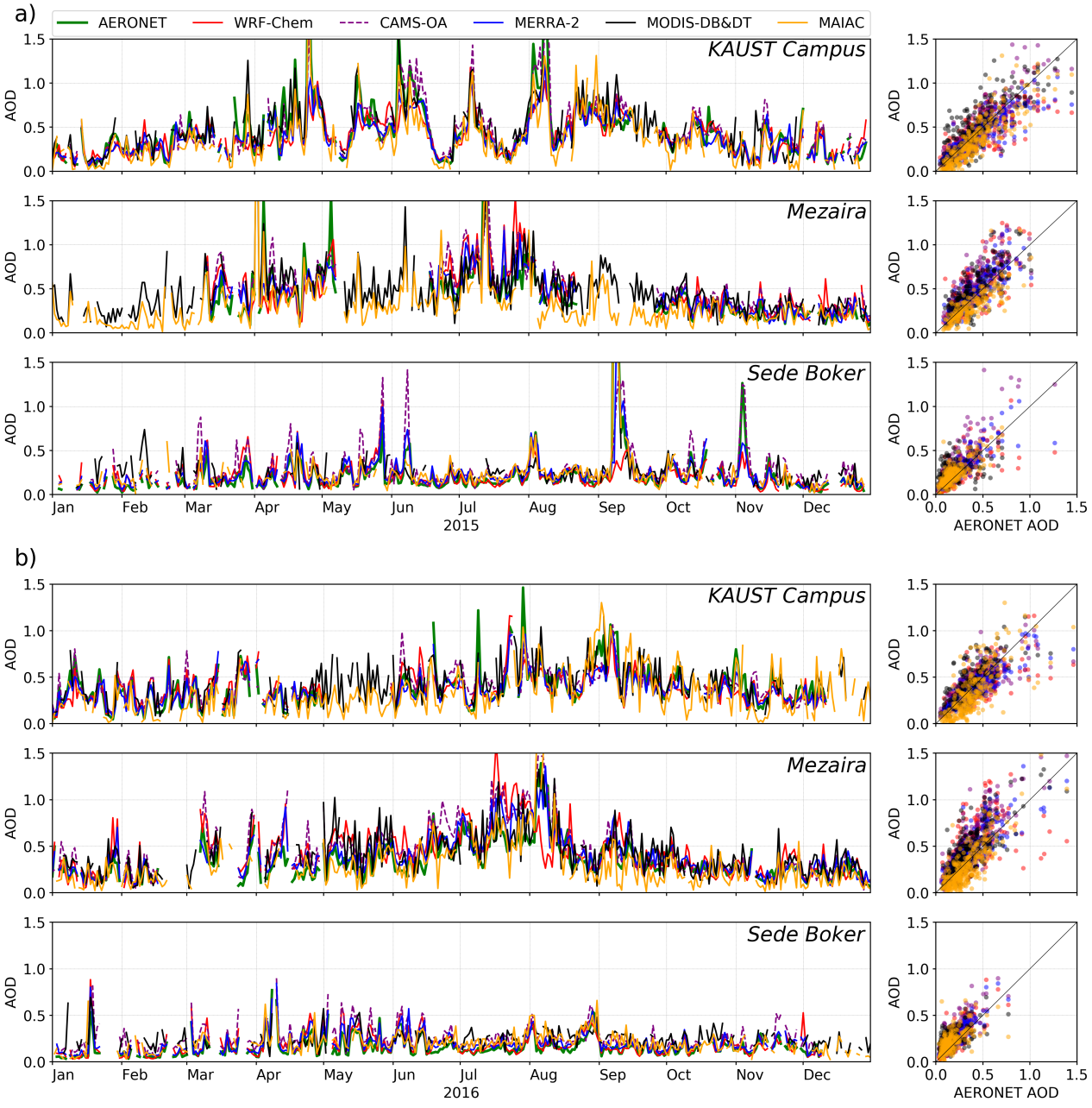

Figure 6. Daily averaged AOD at three AERONET sites (*KAUST Campus, Mezaira, Sede Boker*) and corresponding scatter plots computed for WRF-Chem, AERONET, MERRA-2, CAMS-OA, MODIS-DB&DT, and MAIAC: a) 2015, b) 2016.

385 The scatter plots show that the model and assimilation products are capable of reproducing the magnitude and temporal evolution of the observed AERONET AOD at all sites. During both years, *KAUST Campus* and *Mezaira* sites show higher

AOD in summer and lower AOD in winter. To quantify the capability of the WRF-Chem, MERRA-2, and CAMS-OA models, and the MODIS-DB&DT and MAIAC products to reproduce the AERONET AOD, we calculate Pearson correlation coefficient R and mean bias (see Appendix A2) with respect to the AERONET AOD observations for the 2015-2016 period, see Tab. 4. The correlation coefficients are the highest for MERRA-2 and MAIAC. MAIAC shows better correlation than MERRA-2 during 2015 (0.88-0.96), but MERRA-2 is better correlated with AERONET (0.85-0.91) than MAIAC in 2016. CAMS-OA, despite it does not assimilate AERONET, shows better correlations (0.65-0.87) than MODIS-DB&DT (0.56-0.84). However, CAMS-OA overestimates AOD, particularly during acute dust events, and has a relatively high positive mean bias. The R coefficient for the WRF-Chem AOD is (0.43-0.85). MERRA-2 and WRF-Chem have the lowest mean bias in comparison with the other models and products. MODIS-DB&DT mean bias is positive in 2015 and 2016, while MAIAC mean bias is negative for *KAUST Campus* and *Mezaira* and positive for *Sede Boker* during both years.

We have to mention here that the satellite retrievals and MERRA-2 use AERONET observations for calibration. WRF-Chem is tuned to reduce the annual mean bias with respect to AERONET observations. CAMS-OA does not assimilate AERONET AODs. In WRF-Chem, we did not tune the temporal correlation between the model and AERONET AOD. In this sense, the correlation coefficient between WRF-Chem and AERONET AOD provides an independent evaluation of the model performance (see Tab. 4). It is expected that the temporal correlation for the assimilation products and satellite retrievals will be higher than for the free-running WRF-Chem.

5.2.3 Comparison of spatial AOD distributions

We also examine how well MERRA-2, CAMS-OA, MAIAC, and WRF-Chem reproduce spatial patterns and seasonal variability of the AOD in comparison with the conventional MODIS-DB&DT retrievals. The seasonally and annually-averaged 2015-2016 AOD fields from WRF-Chem, CAMS-OA, MERRA-2, and the two MODIS retrievals DB&DT and MAIAC are presented in Fig. 7. The seasonally averaged AOD's from WRF-Chem, MERRA-2, CAMS-OA are shown at their original spatial resolution and were calculated using only daytime (6 am-2 pm UTC or 9 am-5 pm local time) output. The AODs were sampled under all-sky conditions, which in the ME does not make much of a difference, as cloud fraction is low. For the statistical comparison, we interpolated AOD fields (preserving the area average AODs) on the MERRA-2 grid and calculated the Pearson correlation coefficient R root mean square error $RMSE$ and mean bias with respect to MODIS-DB&DT AOD, see Tab. 5. When conducting statistical analysis, the grid-cells with undefined pixels in MODIS-DB&DT and MAIAC retrievals were excluded.

The statistical scores provided in Tab. 5 show that the annual mean AOD from MAIAC has the highest correlation (R=0.796), but also the highest *RMSE*=0.123, and the biggest bias=-0.095 with respect to MODIS-DB&DT AOD. MERRA-2 annual mean AOD has *R*=0.663 with respect to MODIS-DB&DT AOD, CAMS-OA - *R*=0.650), and WRF-Chem - *R*=0.609 with *RMSE's*=0.116 for all of them. WRF-Chem, MERRA-2, and CAMS-OA demonstrate similar AOD patterns, but WRF-Chem and MERRA-2 underestimate, and CAMS-OA overestimates MODIS-DB&DT AOD during all seasons with the annual mean bias=-0.009, -0.042, 0.039, correspondingly. MAIAC underestimates AOD in comparison with MODIS-DB&DT, which is consistent with the MAIAC and MODIS-DB&DT AOD comparison with AERONET AOD (see Tab. 4 and Fig. 6).

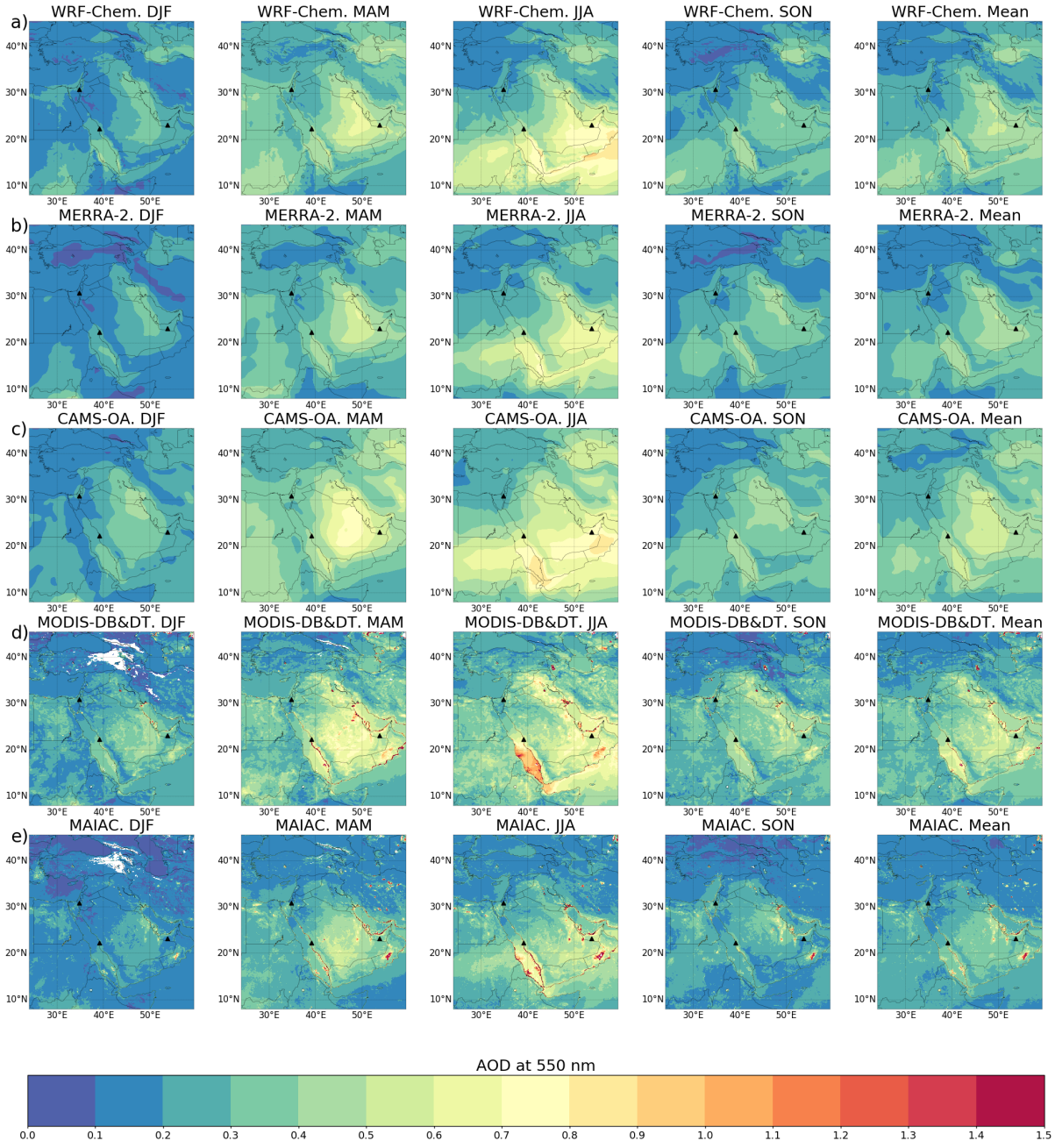

Figure 7. Seasonally averaged 2015-2016 AOD. Right column is annual mean AOD. Rows: a) WRF-Chem, b) MERRA-2, c) CAMS-OA, d) MODIS-DB&DT, and e) MAIAC. Winter (DJF), spring (MAM), summer (JJA), and autumn (SON). White dots are undefined pixels. Black triangles denote locations of *KAUST Campus*, *Mezaira*, and *Sede Boker* AERONET stations.

Table 5. Pearson correlation coefficient (R), root mean square error ($RMSE$) and mean bias calculated for seasonally and annually averaged 2015-2016 AOD geographic distributions from CAMS-OA, MAIAC, MERRA-2, and WRF-Chem with respect to MODIS-DB&DT AOD.

	CAMS-OA			MAIAC			MERRA-2			WRF-Chem		
	R	*RMSE*	*bias*	*R*	*RMSE*	*bias*	*R*	*RMSE*	*bias*	*R*	*RMSE*	*bias*
Winter (DJF)	0.599	0.084	0.019	0.794	0.092	-0.072	0.569	0.090	-0.033	0.473	0.092	-0.008
Spring (MAM)	0.700	0.129	0.052	0.802	0.142	-0.107	0.717	0.127	-0.047	0.661	0.124	-0.007
Summer (JJA)	0.702	0.152	0.069	0.782	0.160	-0.117	0.742	0.133	-0.050	0.685	0.148	0.000
Autumn (SON)	0.559	0.111	0.027	0.717	0.111	-0.084	0.595	0.108	-0.027	0.497	0.116	-0.015
Annual mean	0.650	0.116	0.039	0.796	0.123	-0.095	0.663	0.116	-0.042	0.609	0.116	-0.009

Based on the comparison of WRF-Chem AOD with the AOD from MODIS and AERONET observations, we conclude that spatial and temporal WRF-Chem's AOD distribution is in good agreement with the available satellite and ground-based observations, i.e. annual mean correlation *R* exceeds 0.6 (see Tab. 5) and correlation with AERONET is 0.43-0.85 (see Tab. 4).

5.3 PM air pollution

To test the ability of the data assimilation products and models to characterize PM air pollution in the ME, we compare surface daily mean $PM_{2.5}$ and PM_{10} concentrations from WRF-Chem, MERRA-2, and CAMS-OA, with daily averaged measurements conducted by the three AQMS, see Fig. 8 and 9. The AQMS are installed in Jeddah, Riyadh, and Dammam (Fig. 1), the Saudi Arabian mega-cities. PM measurements conducted by MODON (see Sec. 2.3) are available starting from 2016. The modeled $PM_{2.5}$ and PM_{10} concentrations were sampled from the model fields at the exact AQMS locations. The following formulas were used to calculate $PM_{2.5}$ and PM_{10} surface concentrations using WRF-Chem and MERRA-2 output:

$$\begin{aligned} PM_{2.5} &= DUST_1 + DUST_2 * 0.38 + SEAS_1 + SEAS_2 + SEAS_3 * 0.83 \\ &\quad + \textit{sulfate} + (OC_1 + OC_2) * OC_{mfac} + BC_1 + BC_2 \\ PM_{10} &= DUST_1 + DUST_2 + DUST_3 + DUST_4 * 0.74 + SEAS_1 + SEAS_2 + SEAS_3 + SEAS_4 \\ &\quad + \textit{sulfate} + (OC_1 + OC_2) * OC_{mfac} + BC_1 + BC_2 \end{aligned} \tag{4}$$

where $DUST_{1,2,3,4}$, $SEAS_{1,2,3,4}$, $OC_{1,2}$, $BC_{1,2}$, and $sulfate$ are respectively the concentrations of the dust, and sea-salt in the first four bins, organic and black carbon (hydrophobic and hydrophilic) and sulfate ion (SO_4^{2-}). As was mentioned in Sec. 4.1, $SEAS_1$ is not present in the WRF-Chem output. So for WRF-Chem we assume $SEAS_1$= 0. The factor OC_{mfac} = 1.8 accounts for the conversion of organic carbon into organic matter.

CAMS-OA $PM_{2.5}$ and PM_{10} were calculated using the following relations (https://confluence.ecmwf.int/display/CUSF/PM10+and+PM25+global+products):

$$
\begin{aligned}
PM_{2.5} &= DD_1 + DD_2 + SS_1/4.3 + 0.5 * SS_2/4.3 + 0.7 * (OM_1 + OM_2 + sulfate) + BC_1 + BC_2 \\
PM_{10} &= DD_1 + DD_2 + DD_3 * 0.4 + SS_1/4.3 + SS_2/4.3 + OM_1 + OM_2 + sulfate + BC_1 + BC_2
\end{aligned} \tag{5}
$$

where $DD_{1,2,3}$, $SS_{1,2}$, $sulfate$, $BC_{1,2}$, $OM_{1,2}$ are surface concentration of dust in three bins, sea salt in two bins, sulfate, black carbon, and organic matter (hydrophobic and hydrophilic). The size ranges of dust and sea salt bins from CAMS-OA are presented in Tab. 2.

The histograms at the right-side panels in Fig. 8 and 9 show the annual mean PM concentrations from WRF-Chem, MERRA-2, and CAMS-OA split into the dust and non-dust components. The dashed and dash-dotted horizontal lines correspond to KSA-PME limits and WHO air quality guidelines for daily (on the left-side panels) and annual mean (on the right-side panels) PM concentrations. We also calculated the separate contributions of sulfate, sea salt, organic matter, and black carbon into the non-dust $PM_{2.5}$ and PM_{10}, see Tab. 6 and 7, respectively.

The sporadic peaks in the observations which are not captured by the model and assimilation products are due to unaccounted factors, such as nearby traffic, construction works, and local anthropogenic or natural emissions, which are not present in the emission inventories, or due to meteorological fluctuations that are not resolved in the models. Talking about extreme dust pollution cases, we analyzed dust surface concentrations using WRF-Chem output during the dust storm, which took place in the Jeddah region on 8th July in 2016. The calculated surface concentrations in all dust-bins $DUST_{1,2,3,4,5}$ at the peak of the storm were {55,58,63,111,11} $\mu g/m^3$, respectively. The sum of all dust-bins yields the total dust concentration of 298 $\mu g/m^3$.

5.3.1 $PM_{2.5}$

Fig. 8 shows that the daily averaged $PM_{2.5}$ concentrations observed by MODON AQMS at all locations never drop below the WHO limit of 25 $\mu g/m^3$. During the severe dust events, this limit is exceeded in 2016 10-15 times. The less restrictive KSA-PME limit of 35 $\mu g/m^3$ is exceeded 7-11 times during the dust outbreaks. Annually averaged MODON measurements are 8-18 times higher than the 10 $\mu g/m^3$ WHO limit and 5-12 times higher than the 15 $\mu g/m^3$ KSA-PME limit for annual mean $PM_{2.5}$ concentrations.

Both data assimilation products and WRF-Chem underestimate $\approx$3 times annual mean $PM_{2.5}$ concentrations in Jeddah and Riyadh and slightly overestimate, though WRF-Chem slightly underestimates, $PM_{2.5}$ in Dammam in comparison with observed concentrations during 2016. The CAMS-OA annual mean surface $PM_{2.5}$ concentrations in Jeddah and Riyadh are higher than those from WRF-Chem and MERRA-2, providing the best fit for MODON observations, at least on an annual mean (during 2016) basis.

Annual mean $PM_{2.5}$ concentrations from WRF-Chem and MERRA-2 exceed the WHO limit of 10 $\mu g/m^3$ $\approx$4-7 and $\approx$6-10 times, respectively, in all locations. The KSA-PME limit of 15 $\mu g/m^3$ for annual average $PM_{2.5}$ concentrations is exceeded $\approx$2.5-4.5 and $\approx$4-6.5 times, respectively, for WRF-Chem and MERRA-2.

In Jeddah and Dammam, WRF-Chem and MERRA-2 show similar relative contributions of non-dust components to $PM_{2.5}$ (30-34% in Jeddah and 12-14% in Dammam), but in MERRA-2 sea salt is a major contributor into non-dust $PM_{2.5}$, while

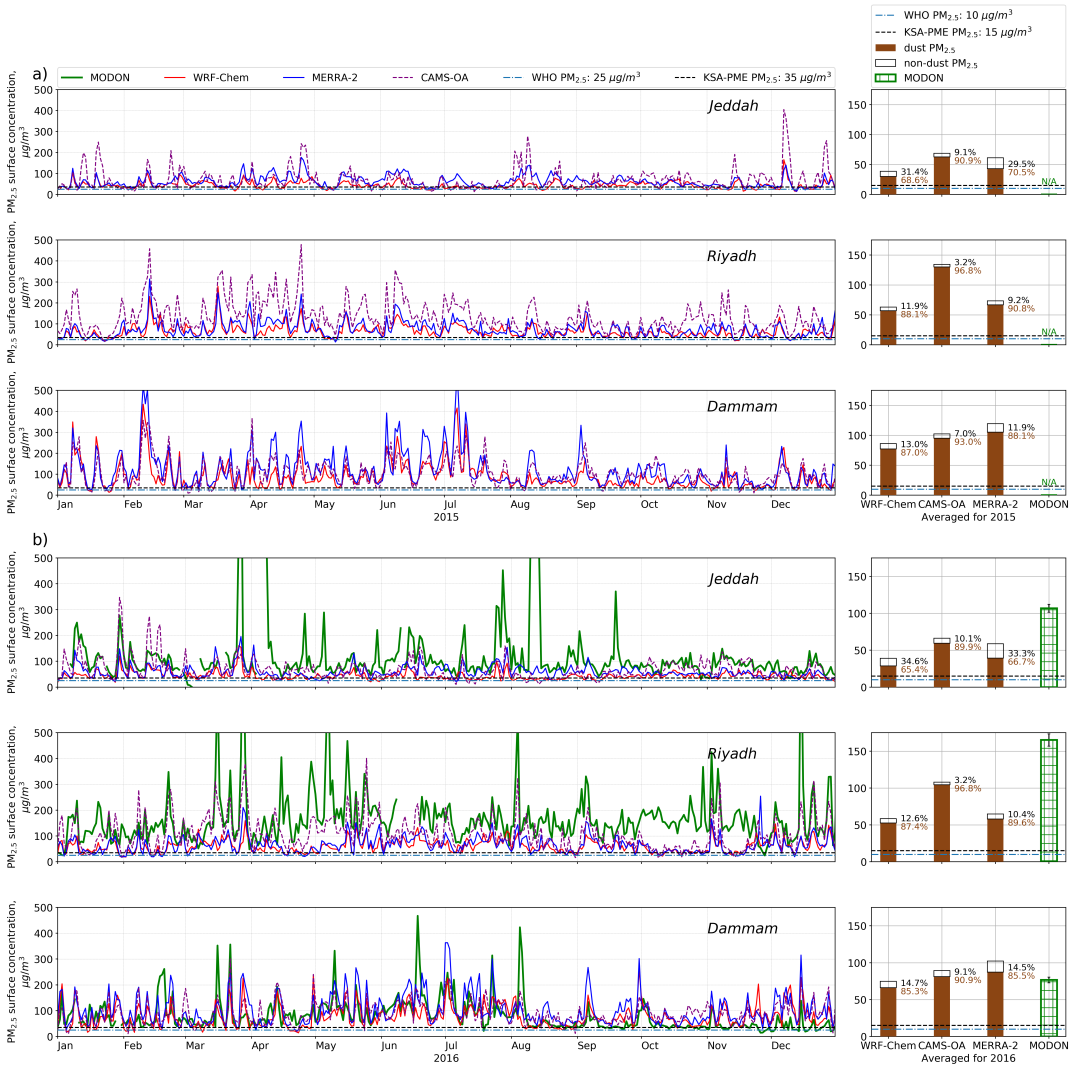

Figure 8. Left: WRF-Chem daily averaged $PM_{2.5}$ surface concentrations ($\mu g/m^3$) with MODON observations, MERRA-2, CAMS-OA at Jeddah, Riyadh, Dammam. The dash-dotted line corresponds to the 25 $\mu g/m^3$ WHO daily average guideline. Right: stacked bars show the decomposition of the $PM_{2.5}$ annual mean surface concentrations into dust and non-dust components. The dash-dotted line corresponds to the 10 $\mu g/m^3$ WHO annual guideline. Numbers on the right hand side of WRF-Chem, CAMS-OA, and MERRA-2 bars show the contribution (%) of the dust and non-dust into the total $PM_{2.5}$ concentration. a) 2015, b) 2016.

in WRF-Chem it is sulfate, see Tab. 6. This difference between WRF-Chem and MERRA-2 is mainly because MERRA-2 generates more sea salt, but also because MERRA-2 underestimates SO_2 emissions located in the Arabian Gulf and along the west coast of Saudi Arabia (Ukhov et al., 2020b), and hence underestimates sulfate concentrations, as discussed in Sec. 4.1. In Riyadh, the contribution of the non-dust component to $PM_{2.5}$ is ≈9-12% for both MERRA-2 and WRF-Chem. In CAMS-OA,

the contribution of non-dust particulates to $PM_{2.5}$ in Jeddah and Dammam is ≈7-10%, and the contribution of sea salt is little. According to Tab. 6, in all considered cities, the contribution of black carbon (BC) to $PM_{2.5}$ is not significant for all models. In MERRA-2, the contribution of organic matter (OM) to $PM_{2.5}$ is more substantial (but still minor) in comparison with WRF-Chem and CAMS-OA. In general, among all models contribution of dust to $PM_{2.5}$ in Jeddah is 65-90%, while in Riyadh and Dammam this contribution is 85-95%, see Tab. 6.

Table 6. Contributions (%) of dust and non-dust components into $PM_{2.5}$ for Jeddah, Riyadh, and Dammam during 2015-2016.

	Jeddah			Riyadh			Dammam		
	WRF-Chem	CAMS-OA	MERRA-2	WRF-Chem	CAMS-OA	MERRA-2	WRF-Chem	CAMS-OA	MERRA-2
	2015								
dust	68.6	90.9	70.6	88.1	96.8	90.8	87.0	93.0	88.1
sulf	19.9	5.1	6.1	9.0	2.1	5.0	10.0	3.9	3.6
BC	2.1	0.7	0.6	0.1	0.2	0.3	0.1	0.7	0.3
OM	4.0	3.1	5.1	1.8	0.8	2.7	1.5	2.3	3.1
salt	5.5	0.1	17.6	0.8	0.1	1.3	1.3	0.1	4.9
	2016								
dust	65.4	89.9	66.8	87.4	96.8	89.6	85.3	90.9	85.5
sulf	23.2	5.7	6.8	9.5	1.9	5.7	11.3	4.7	4.3
BC	2.1	0.8	0.7	0.2	0.3	0.3	0.2	0.9	0.4
OM	4.0	3.4	5.4	2.1	0.9	2.9	1.8	3.4	4.1
salt	5.4	0.1	20.4	0.9	0.1	1.4	1.5	0.1	5.7

* for WRF-Chem and MERRA-2: $dust = DUST_1 + DUST_2 * 0.38$, $BC = BC_1 + BC_2$, $sulf = sulfate$, $OM = (OC_1 + OC_2) * OC_{mfac}$, $salt = SS_1 + SS_2 + SS_3 * 0.83$

** for CAMS: $dust = DD_1 + DD_2$, $sulf = 0.7 * sulfate$, $BC = BC_1 + BC_2$, $OM = 0.7 * (OM_1 + OM_2)$, $salt = SS_1/4.3 + 0.5 * SS_2/4.3$

Abbreviations of the aerosols' names correspond to those given in Sec. 5.3.

5.3.2 PM_{10}

Daily averaged MODON measurements almost continuously exceed the WHO guideline of 50 $\mu g/m^3$ at all locations, see Fig. 9. In Riyadh and Dammam, PM_{10} concentration is higher than in Jeddah, where the KSA-PME limit of 340 $\mu g/m^3$ for daily averaged PM_{10} is exceeded in 2016 about a dozen times. In Dammam, this limit is more frequently exceeded, especially during the summer period. During acute dust events in Dammam, daily averaged PM_{10} concentrations can exceed the WHO guideline limit by more than 10-20 times. Annually averaged MODON measurements are 7-11 times higher than the 20 $\mu g/m^3$ WHO guideline, and in 2-3 times higher than the 80 $\mu g/m^3$ KSA-PME limits for annual mean PM_{10} concentrations.

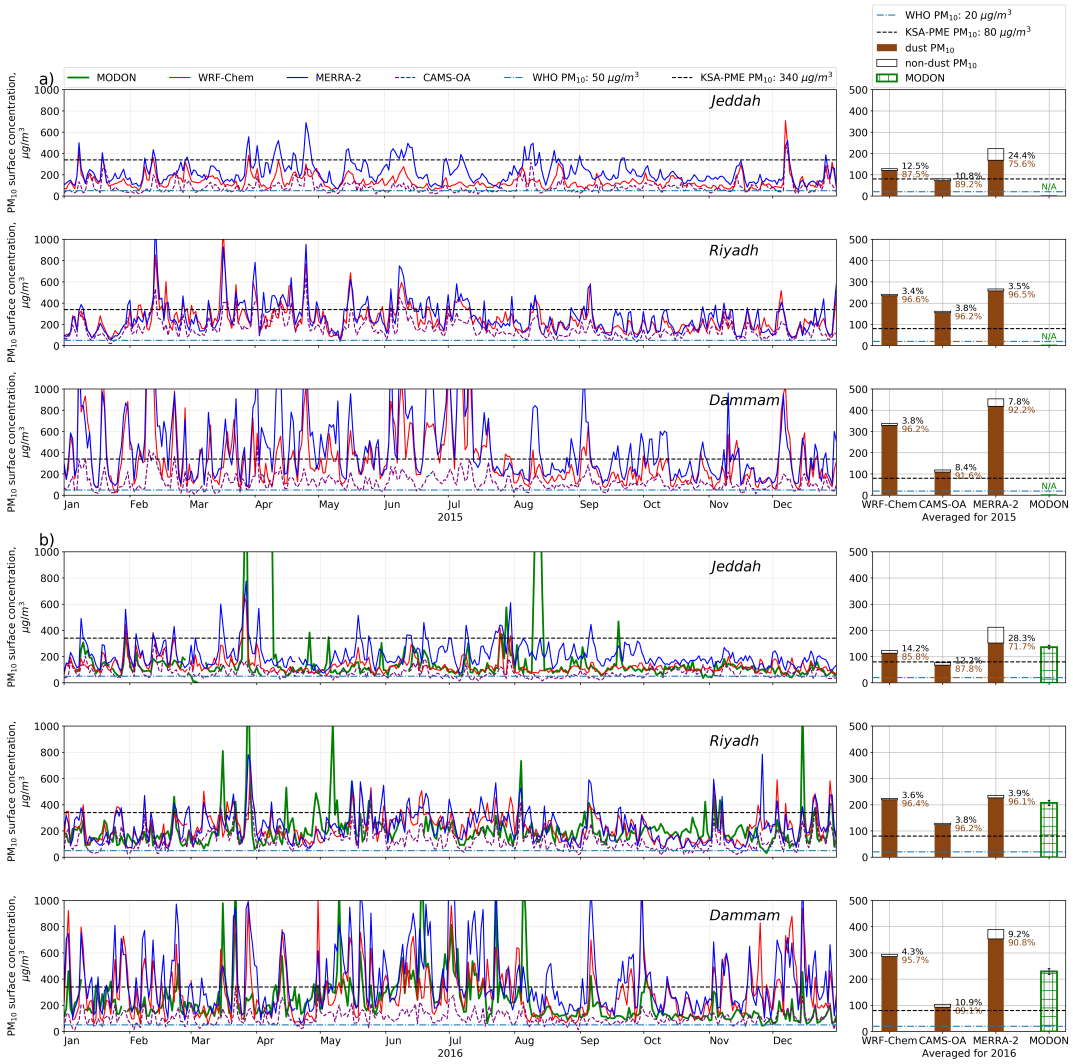

Figure 9. Left: WRF-Chem daily averaged PM_{10} surface concentrations ($\mu g/m^3$) with the MODON observations and MERRA-2 and CAMS-OA, at Jeddah, Riyadh, and Dammam. The dash-dotted line corresponds to the 50 $\mu g/m^3$ WHO daily - guideline. Right: stacked bars show the decomposition of the PM_{10} annual mean surface concentrations into dust and non-dust components. The dash-dotted line corresponds to the 20 $\mu g/m^3$ WHO annual guideline. Numbers on the right-hand side of WRF-Chem, CAMS-OA, and MERRA-2 bars show the contribution (%) of the dust and non-dust particulates to the total PM_{10} concentration. a) 2015, b) 2016 year.

In contrast with MERRA-2 and CAMS-OA, WRF-Chem compares better with PM_{10} observations by MODON in all locations. MERRA-2 overestimates ≈1.2-1.8 times and CAMS-OA underestimates ≈1.5-2 times annual mean PM_{10} MODON observations in all locations. This is in agreement with Cuevas et al. (2014), who stated that MACC (the predecessor of CAMS-OA) underestimates PM_{10} daily and monthly means all year long, and with our findings in Sec. 5.2.1, where we have shown that

CAMS-OA underestimates the volume of particles with radii 0.9-20 μm. Annual mean PM_{10} concentrations from WRF-Chem and MERRA-2 exceed the WHO limit of 20 $\mu g/m^3$ ≈6-15 and ≈10-20 times, respectively, in all locations. The KSA-PME limit of 80 $\mu g/m^3$ for annual average PM_{10} concentrations is exceeded ≈1.5-4 and ≈1.5-5 times, respectively, for WRF-Chem and MERRA-2.

According to Tab. 7 MERRA-2 shows the highest contribution of the sea salt into PM_{10} in the coastal cities of Jeddah (≈21-25%) and Dammam (≈6-7%). MERRA-2 demonstrates the lowest (≈1-2%) contribution of sulfate to PM_{10}, while WRF-Chem and CAMS-OA produce similar sulfate contribution to PM_{10} in Jeddah ((≈7%)) and Riyadh ((≈2.4%)). MERRA-2 also shows the lowest contribution (≈0.1-0.2%) of black carbon (BC) to PM_{10} in all considered cities. CAMS-OA organic matter (OM) contribution to PM_{10} is prevailing in 2-8 times over the WRF-Chem and MERRA-2 contributions. CAMS-OA demonstrates the lowest (0.1-0.2%) contribution of sea salt to PM_{10}. Contribution of dust to PM_{10} in Jeddah is 70-90%, while in Riyadh and Dammam this contribution is 90-96%. Minimal contribution (≈3.5-4%) of non-dust components to PM_{10} is observed among all models in Riyadh.

Table 7. Contributions (%) of dust and non-dust components into PM_{10} for Jeddah, Riyadh, and Dammam during 2015-2016.

	Jeddah			Riyadh			Dammam		
	WRF-Chem	CAMS-OA	MERRA-2	WRF-Chem	CAMS-OA	MERRA-2	WRF-Chem	CAMS-OA	MERRA-2
	2015								
dust	87.5	89.2	75.6	96.6	96.2	96.5	96.2	91.6	92.2
sulf	6.3	6.2	1.7	2.4	2.6	1.4	2.6	4.8	0.9
BC	0.7	0.6	0.2	0.0	0.2	0.1	0.0	0.6	0.1
OM	1.3	3.8	1.4	0.5	1.0	0.7	0.4	2.8	0.8
salt	4.2	0.2	21.2	0.5	0.1	1.4	0.8	0.2	6.0
	2016								
dust	85.8	87.8	71.7	96.4	96.2	96.1	95.7	89.1	90.8
sulf	7.8	7.0	1.9	2.5	2.3	1.6	2.9	5.7	1.1
BC	0.7	0.7	0.2	0.0	0.2	0.1	0.0	0.8	0.1
OM	1.3	4.2	1.5	0.5	1.1	0.8	0.5	4.2	1.1
salt	4.4	0.2	24.8	0.5	0.1	1.5	0.9	0.2	6.8

* for WRF-Chem and MERRA-2: $dust = DUST_1 + DUST_2 + DUST_3 + DUST_4 * 0.74$, $sulf = sulfate$, $BC = BC_1 + BC_2$, $OM = (OC_1 + OC_2) * OC_{mfac}$, $salt = SS_1 + SS_2 + SS_3 + SS_4$

** for CAMS: $dust = DD_1 + DD_2 + DD_3 * 0.4$, $sulf = sulfate$, $BC = BC_1 + BC_2$, $OM = OM_1 + OM_2$, $salt = SS_1/4.3 + SS_2/4.3$

Abbreviations of the aerosols' names correspond to those given in Sec. 5.3.

5.3.3 Spatial patterns of PM air pollution

In this section we use WRF-Chem output averaged for 2015-2016 to discuss the spatial patterns of aerosol pollution and partial contributions from natural and anthropogenic aerosols into PM over the ME.

Figures 10 a, b, c show the spatial distributions of the $PM_{2.5}$ and PM_{10} surface concentrations and the $PM_{2.5}/PM_{10}$ ratio. The left limits of the color bars for $PM_{2.5}$ and PM_{10} are set to be equal to the corresponding WHO annual guideline concentrations. Over the whole domain, the annual mean surface concentrations of $PM_{2.5}$ and PM_{10} exceed WHO guidelines of 10 and 20 $\mu g/m^3$, correspondingly. The regions of high surface concentrations coincide with the main dust sources, which span from Northern Iraq to Oman, include Sudan, Egypt, Libya, and Turkmenistan. PM concentrations in these regions exceed even the less restrictive KSA-PME air quality limit for annual mean $PM_{2.5}$ and PM_{10} concentrations by more than 5 times.

In the entire domain, the max, min, and mean values of the $PM_{2.5}/PM_{10}$ ratio (see Fig. 10c) are 0.73, 0.20, and 0.31 respectively. As expected, the lower $PM_{2.5}/PM_{10}$ ratios (0.2-0.3) are observed over the dust source regions (i.e., along the eastern Arabian peninsula, Iraq, and northern Africa), where both coarse and fine particles are generated. However, large particles can not be transported as far from source regions as small particles, due to the shorter lifetime of large particles compared with small particles with respect to deposition processes. The higher values (0.4-0.6) of the $PM_{2.5}/PM_{10}$ ratio are observed over south-eastern Europe, Turkey, Ethiopia, and western parts of the Arabian Peninsula that are farther from the main dust sources.

Figure 10d shows the sum of surface concentrations of organic matter and black carbon $(OC_1 + OC_2) * OC_{mfac} + BC_1 + BC_2)$. Their max, min, and mean concentration values are 31.8, 0.2, and 1.3 $\mu g/m^3$ respectively. Their contribution to aerosol pollution over the Arabian Peninsula in WRF-Chem simulations is insignificant. Figure 10e shows the surface concentration of sea salt calculated as a sum of concentrations in each bin $SEAS_2 + SEAS_3 + SEAS_4$. Over the seas and coastal areas, the average concentration of sea salt is 3-12 $\mu g/m^3$. In summer, strong winds in *Somali jet* (see Fig. 3b intensify sea salt emission over the Arabian Sea, creating high surface concentrations of sea salt (27-42 $\mu g/m^3$) along the coasts of Somalia and Oman. Due to prevailing northern winds, the transport of sea salt from the Mediterranean Sea to Egypt and Libya is observed.

The relatively high sulfate surface concentration (see Fig. 10f) is observed in the vicinity of the strong SO_2 sources located along the west and east coast of Saudi Arabia and over the Arabian Gulf, as well as downwind from those sources, see (Ukhov et al., 2020b) for details. Figure 10f also denotes the locations of the AERONET stations, as in Fig. 1. The sulfate concentration at the *KAUST Campus* site is higher than at the *Mezaira* and *Sede Boker* AERONET sites (see Sec. 5.2.1) so it experiences more pronounced contribution of sulfate particulates into the fine mode of the AVSD (see Fig. 4a and Fig. 5). Due to the prevailing northern winds along the Red Sea, sulfate aerosols originating from SO_2 emissions along the Red Sea coast spread along the west coast of the Arabian Peninsula towards Yemen. The drift of sulfate from the Arabian Gulf into the interior of the Eastern part of the Arabian Peninsula is also seen. The sulfate annual mean background surface concentration over the US for the period 2003–2012, obtained in Buchard et al. (2016), is 2-3 $\mu g/m^3$, similar to the background concentrations we see in the ME. But in the downwind or in the vicinity of strong SO_2 point emissions, sulfate concentrations are 3-4 times higher. Similar sulfate surface concentrations for the period 2000-2016 over the US were obtained in van Donkelaar et al. (2019), where the

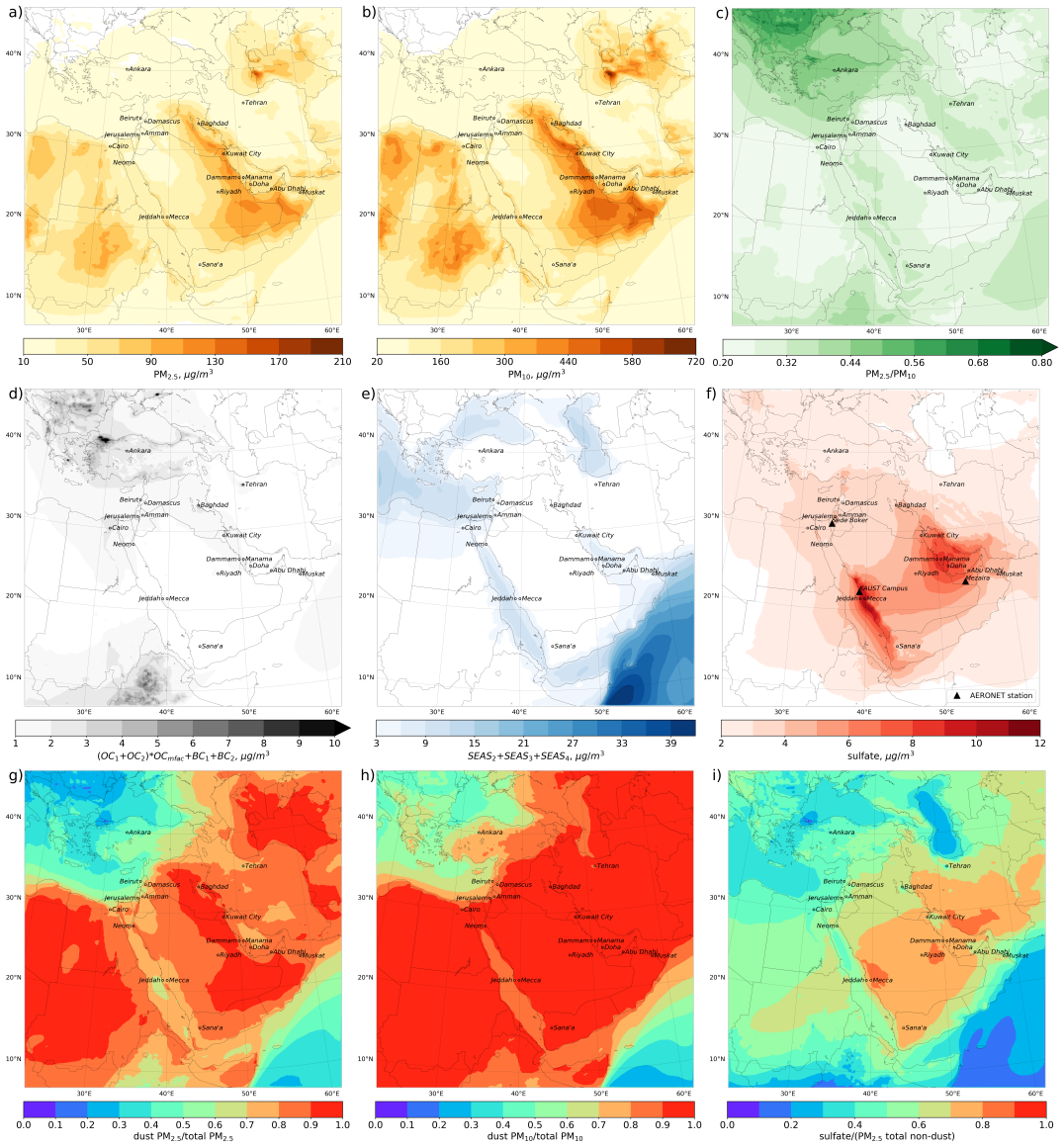

Figure 10. WRF-Chem's average 2015-2016 surface concentrations, ($\mu g/m^3$): a) $PM_{2.5}$, b) PM_{10}; c) ratio $PM_{2.5}/PM_{10}$; d) black carbon and organic matter ($(OC_1 + OC_2) * OC_{mfac} + BC_1 + BC_2$), ($\mu g/m^3$), e) sea salt ($SEAS_2 + SEAS_3 + SEAS_4$), ($\mu g/m^3$), f) sulfate, ($\mu g/m^3$) and locations of AERONET stations, g) ratio dust $PM_{2.5}$/(total $PM_{2.5}$), h) ratio dust PM_{10}/(total PM_{10}), i) ratio sulfate/($PM_{2.5}$ total non-dust). Abbreviations of the aerosols' names correspond to those given in Sec. 5.3.

concentrations reach ≈10 $\mu g/m^3$ over the eastern part of the US during summer. In Al-Taani et al. (2019) the average 1980-2016 sulfate concentration computed for UAE is 2.5-3 times lower. This difference is caused by the fact that Al-Taani et al.

(2019) took the sulfate fields from MERRA-2 reanalysis, which underestimates the SO_2 emissions as shown in (Ukhov et al., 2020b).

Contributions of dust to $PM_{2.5}$ and PM_{10} calculated as ratios of dust $PM_{2.5}$ to total $PM_{2.5}$, and dust PM_{10} to total PM_{10}, are shown in Fig. 10g and 10h, respectively. Due to relatively low dust surface concentrations over the eastern Mediterranean, Turkey, and south-eastern Europe, the contribution of dust to $PM_{2.5}$ and PM_{10} is 20-50% and 50-80%, respectively. In other areas that are closer to the dust source regions, the contribution of dust to PM is above 80%.

Figure 10i shows the ratio between the concentration of sulfate aerosol with respect to the total concentration of $PM_{2.5}$ non-dust aerosols. The max, min, and mean values of this ratio are 0.84, 0.07, and 0.52, respectively. This ratio is low over the seas where sea salt is prevalent but consistently exceeds 0.6 over land. Sulfate, therefore, is the primary anthropogenic pollutant over land. In the central and southern parts of Saudi Arabia, and over Iran, sulfate contributes 60-90% to the total $PM_{2.5}$ non-dust aerosols concentration. Over the other parts of the Arabian Peninsula, the northern part of Sudan, Libya, and Egypt, sulfate contributes approximately 40-60% to total $PM_{2.5}$ non-dust aerosols concentration.

5.3.4 PM air pollution in the ME major cities

To evaluate the air-quality in the ME's major cities, we calculate for their locations the average for 2015-2016 daily $PM_{2.5}$ and PM_{10} surface concentrations, their 90th percentiles, and we also calculate the contribution of the dust and non-dust components into PM (see Fig. 11). We calculate the number of days during the 2015-2016 period when the daily $PM_{2.5}$ and PM_{10} surface concentrations exceed the US-EPA air-quality limit of 35 $\mu g/m^3$ and 150 $\mu g/m^3$ respectively.

Figure 11 shows that the annually-averaged $PM_{2.5}$ and PM_{10} exceed the WHO air-quality guidelines 2-9 and 3-20 times, respectively in all major cities of the ME, except Ankara. The KSA-PME air-quality limit for annual mean $PM_{2.5}$ is exceeded by up to 6 times, and by up to 5 times for PM_{10}. Due to the lack of strong dust sources nearby, air-quality conditions in the cities in the eastern Mediterranean are more favorable when compared with those in the Arabian Peninsula. In these cities, the air pollution shifts from natural to anthropogenic, as the contribution of non-dust aerosols to $PM_{2.5}$ increases up to 30-45%, in contrast with the cities located in the Arabian Peninsula, where this contribution is up to 8-25%. Sulfate aerosol is the major contributor to non-dust $PM_{2.5}$.

The cities at the eastern coast of the Arabian Peninsula have the highest 90th percentiles of daily mean PM concentrations. For example, in Dammam, Abu Dhabi, Doha, and Kuwait City, the 90th percentiles of daily mean surface concentration of PM_{10} and $PM_{2.5}$ are in the range of 400-740 and 130-180 $\mu g/m^3$ respectively. This is above the KSA-PME air-quality limits for daily mean PM_{10} and $PM_{2.5}$.

In the Eastern Mediterranean cities, within the 2015-2016 period, the US-EPA air-quality daily mean limits are exceeded 40-75 days for PM_{10} and 60-100 days for $PM_{2.5}$. In the cities of the Arabian Peninsula, Iraq, and Iran, the US-EPA PM daily mean limits are exceeded 94-627 days for PM_{10} and 213-640 days for $PM_{2.5}$ during the same period.

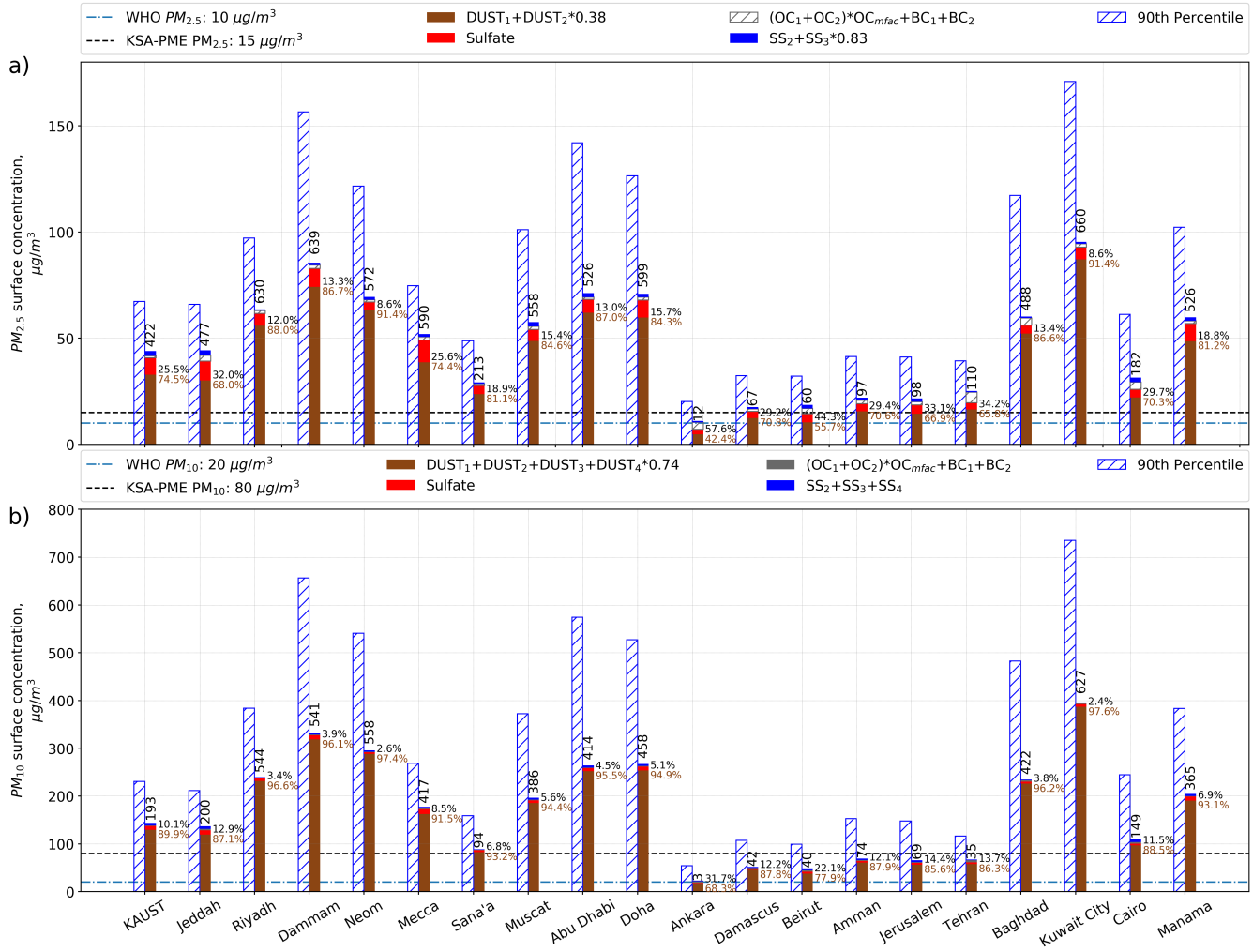

Figure 11. Annual mean 2015-2016 PM surface concentrations ($\mu g/m^3$) calculated for the ME major cities and PM decomposition into dust and non-dust (sulfate, sea salt, black carbon and organic matter) components (stacked bars). Abbreviations of the aerosols' names correspond to those given in Sec. 5.3. Hatched bars denote 90th percentiles ($\mu g/m^3$) calculated using daily mean PM concentrations. WHO guidelines and KSA-PME air-quality limits for annual averaged PM are shown by dash-dotted and dashed lines. Numbers over the stacked bars correspond to the number of days during 2015-2016, when daily averaged PM surface concentration exceeded US-EPA air-quality limit: a) $PM_{2.5}$. Daily averaged US-EPA air-quality limit is 35 $\mu g/m^3$. Annual WHO guideline and KSA-PME limit are 10 and 15 $\mu g/m^3$, respectively; b) PM_{10}. Daily averaged US-EPA air-quality limit is 150 $\mu g/m^3$. Annual WHO and KSA-PME limits are 20 and 80 $\mu g/m^3$, respectively.

6 Conclusions

This study ~~assesses the impact of aerosols on air pollution in the Middle East. It presents an evaluation of two aerosol~~ evaluates MERRA-2 and CAMS-OA data assimilation products, ~~MERRA-2 and CAMS-OA, as well as~~ and high-resolution WRF-Chem simulations aiming at assessing the impact of aerosols on PM air pollution over the Middle East ~~. In the scope of this study, we conducted high-resolution WRF-Chem simulations~~ for the 2015-2016 period. ~~We evaluated the AOD and PM air pollution over the Arabian Peninsula and in the ME major cities. We also tested~~ It also compares the new MODIS AOD retrieval, MAIAC, with the conventional MODIS-DB&DT and AERONET AOD over the Middle East ~~.~~

~~The WRF-Chem v3.7.1 code was fixed to describe the aerosol effects correctly, and~~ major dust source regions. MERRA-2 ~~has been used for constructing boundary and initial conditions for meteorological and chemistry/aerosol variables. To improve the calculation of sulfate aerosols, the most accurate emission dataset retrieved from OMI observations using the "top-down" approach was implemented in WRF-Chem calculations. We also tuned in WRF-Chem the dust emission size distribution to match the retrieved AERONET AVSDs.~~

~~MERRA-2~~ and WRF-Chem use the five-bin ~~GOCART~~ dust aerosol model and demonstrate a better agreement with the AERONET ~~observations~~ retrieved size distribution than CAMS-OA~~that~~ , which uses a three dust-bins microphysical model. CAMS-OA overestimates the volume of fine dust particles with radii of 0.55-0.9 μm and underestimates the volume of coarse dust particles with radii of 0.9-20 μm in comparison with the AERONET aerosol volume size distribution.

At all considered AERONET sites, WRF-Chem, CAMS-OA, MERRA-2, MODIS-DB&DT, and MAIAC ~~can reproduce~~ are capable of reproducing the magnitude and temporal evolution of the AERONET AOD time series during the whole period. MAIAC and MERRA-2 have the highest correlation to AERONET AOD. CAMS-OA ~~shows better correlation than MODIS-DB&DT, although CAMS-OA overestimates~~ tends to overestimate AERONET AOD, especially during ~~the~~ severe dust events~~and exhibits a relatively high positive bias~~. The MODIS-DB&DT and MAIAC ~~retrieval products have similar absolute values of the mean bias, which is~~ AOD mean biases with respect to AERONET observations are of the same magnitude (slightly larger than that of MERRA-2~~and WRF-Chem. The~~), but the MODIS-DB&DT AOD is biased positively, ~~but~~ and the MAIAC AOD is biased negatively except for *Sede Boker* for both years. The ~~spatial~~ AOD fields from WRF-Chem and assimilation products exhibit similar spatial patterns, but WRF-Chem, MAIAC, and MERRA-2 underestimate, and CAMS-OA overestimates MODIS-DB&DT AOD. MAIAC has the highest ~~correlation~~spatial correlation to the conventional MODIS-DB&DT AOD, followed by MERRA-2, CAMS-OA, and WRF-Chem.

The capability of WRF-Chem, MERRA-2, and CAMS-OA in reproducing PM air pollution over the ~~ME~~ Middle East was tested against *in situ* measurements. These PM measurements are conducted in the industrial regions of Jeddah, Riyadh, and Dammam, which complicates one-to-one comparison with the output from global and regional models. Annual mean PM concentrations from WRF-Chem and MERRA-2 exceed the ~~corresponding WHO limits up to~~ WHO limit almost 20 times. The KSA-PME limit for annual average concentrations is ~~exceeded up to 6.5 times. The CAMS-OA annual mean $PM_{2.5}$ fits the MODON AQMS observations better than other products. CAMS-OA,~~ also exceeded more than 6 times. MERRA-2 ~~,~~ and WRF-Chem underestimate ~~≈3 times~~ the observed annual mean $PM_{2.5}$ ~~observed~~ concentrations during 2016 in Jeddah and

Riyadh almost 3 times. CAMS-OA, MERRA-2 overestimate, and WRF-Chem underestimates observed annual mean $PM_{2.5}$ in Dammam. ~~In Jeddah and Dammam, WRF-Chem and MERRA-2 show similar relative contributions of non-dust components to $PM_{2.5}$. Still, in MERRA-2, sea salt is a major contributor in non-dust aerosol concentration, while in WRF-Chem, it is a sulfate. This difference is both because MERRA-2 generates more sea salt and underestimates emissions, hence underestimating sulfate concentrations. In Jeddah, Dammam, and Riyadh, the contribution of black carbon to $PM_{2.5}$ is insignificant for all models. WRF-Chem results compare better with PM_{10} MODON observations in all locations than ones from MERRA-2 and~~ CAMS-OA ~~. MERRA-2 overestimates ≈1.2-1.8 times. CAMS-OA underestimates ≈~~underestimates (1.5-2 times) annual mean PM_{10} ~~MODON~~ observations in all locations primarily due to its ~~deficiency in the~~ deficient dust size distribution. ~~MERRA-2 shows the highest contribution of the sea salt and the lowest contribution of black carbon and sulfate to PM_{10} in all locations.~~ The CAMS-OA ~~organic matter contribution to PM_{10} is prevailing over the WRF-Chem and MERRA-2 contributions. CAMS-OA demonstrates the lowest contribution of sea salt to PM_{10}. Minimal contribution of non-dust components to PM_{10} is observed among all models in Riyadh.~~ annual mean $PM_{2.5}$ fits the PM observations better than other products.

The PM composition analysis over rural areas shows that in WRF-Chem, the annual average $PM_{2.5}/PM_{10}$ ratio over the ME is about 0.3. It decreases to 0.25 over the major dust source regions, i.e., in the eastern Arabian peninsula, Iraq, and northern Africa. In most parts of the ~~ME~~Middle East, dust is the major contributor to PM. The sulfate aerosol contribution to $PM_{2.5}$ is essential in the areas where strong SO_2 sources are present, i.e., in the west and east coasts of Saudi Arabia and over the Arabian Gulf. In these areas sulfate surface concentration reaches 8-11 $\mu g/m^3$, while the "clean" background level is 2-4 $\mu g/m^3$. High sulfate content along the west coast of Saudi Arabia is consistent with the increased volume of the fine mode in the *KAUST Campus* AERONET ~~AVSD~~ site in comparison with ~~AVSDs from other~~ *Mezaira* and *Sede Boker* sites. In WRF-Chem, sulfate is the major non-dust pollutant over the ~~ME~~Middle East. Sulfate aerosols contribute 60-90 % to the total $PM_{2.5}$ non-dust aerosols over the central and southern parts of Saudi Arabia and Iran. Over the other parts of the Arabian Peninsula, northern Sudan, Libya, and Egypt, sulfate contributes approximately 40-60 % to the total $PM_{2.5}$ non-dust aerosol concentration. ~~In Jeddah and Dammam, WRF-Chem and MERRA-2 show similar relative contributions of the non-dust component to $PM_{2.5}$ (30-34% in Jeddah and 12-14% in Dammam). In MERRA-2, in contrast with WRF-Chem, sea salt is a major non-dust contributor to $PM_{2.5}$. In CAMS-OA contribution of the non-dust particulates to $PM_{2.5}$ in Jeddah and Dammam is ≈7-10% and the contribution of sea salt is little. In Riyadh, the contribution of the non-dust component to $PM_{2.5}$ is ≈9-12% for both MERRA-2 and WRF-Chem.~~

The analysis of the annually averaged $PM_{2.5}$ and PM_{10} surface concentrations in the ~~ME~~ Middle East major cities shows a very high PM pollution level. In Dammam, Abu Dhabi, Doha, and Kuwait City, the 90th percentile of PM_{10} and $PM_{2.5}$ annual mean surface concentrations exceed 400-740 and 130-180 $\mu g/m^3$ respectively, which is above the KSA-PME air-quality limit. In the eastern Mediterranean, dust concentration drops, and non-dust aerosols' contribution to $PM_{2.5}$ increases up to 30-45%. In the cities located in the Arabian Peninsula contribution of the non-dust component to $PM_{2.5}$ is 8-25%, which limits the effect of the emission control on air-quality. In the eastern Mediterranean cities during the 2015-2016 period, the daily mean surface PM concentrations exceed the US-EPA air quality daily mean limit 40-75 days for PM_{10} and 60-100 days for $PM_{2.5}$. In the ~~ME~~ major cities over the Arabian peninsula, Iraq, and Iran, the US-EPA air-quality daily mean limit is exceeded 94-627 days for PM_{10} and 213-640 days for $PM_{2.5}$. In Jeddah and Dammam, WRF-Chem and MERRA-2 show similar relative

contributions of the non-dust component to $PM_{2.5}$ (30-34% in Jeddah and 12-14% in Dammam). But in MERRA-2, sea salt is a major contributor in non-dust aerosol concentration, while in WRF-Chem, it is a sulfate. This difference is both because MERRA-2 generates more sea salt and underestimates SO_2 emissions and, consequently, sulfate concentrations. In CAMS-OA contribution of non-dust particulates to $PM_{2.5}$ in Jeddah and Dammam is ≈7-10% and the contribution of sea salt is little. In Riyadh, the contribution of the non-dust component to $PM_{2.5}$ is ≈9-12% for both MERRA-2 and WRF-Chem. In Jeddah, Dammam, and Riyadh, the contribution of black carbon to $PM_{2.5}$ is insignificant for all products. MERRA-2 shows the highest contribution of sea salt and the lowest contribution of black carbon and sulfate to PM_{10} in all locations. CAMS-OA demonstrates the lowest contribution of sea salt to PM_{10}. The minimum contribution of non-dust components to PM_{10} is observed in Riyadh among all models.

Thus, in this study, we found that MERRA-2 and CAMS-OA assimilation products, as well as WRF-Chem output despite some intrinsic uncertainties, could be used for evaluation the PM air pollution over the ME. All products show the dominant contribution of mineral dust into PM. However, in the Arabian coastal areas where SO_2 emissions are high, both contributions of sulfate and sea salt could be significant. The broad effect of natural aerosols on air quality in the ME puts stricter requirements on anthropogenic pollution control. The impact of dust could be alleviated by employing specific to desert areas architectural solutions, increasing in-city vegetation cover, and providing air-quality forecasts to alarm the population on hazardous air quality. The developed WRF-Chem modeling framework can be used to simulate other pollutants like NO_x and O_3. The results of the current research could serve as ~~the~~ a basis for an improved air-quality forecast system that interactively calculates high-resolution radiative, dynamical, atmospheric chemistry and aerosol processes, driven by natural and anthropogenic emissions. This system will be especially valuable for the prediction of extreme pollution events. It will also improve understanding of the impact of anthropogenic and natural pollution on air quality and human health in the ME region.

Code availability.

1. *Merra2BC* interpolation utility is available at http://github.com/saneku/Merra2BC

Data availability.

1. MERRA-2 data are available at https://disc.gsfc.nasa.gov/daac-bin/FTPSubset2.pl
2. CAMS-OA data are available at http://apps.ecmwf.int/datasets/data/cams-nrealtime
3. MODIS-DB&DT AOD level 2 data are available at https://ladsweb.modaps.eosdis.nasa.gov/about/purpose
4. AERONET data are available at https://aeronet.gsfc.nasa.gov/
5. MAIAC data are available at https://lpdaac.usgs.gov/products/mcd19a2v006/
6. HTAP-2.2 emission inventory is available at http://edgar.jrc.ec.europa.eu/htap_v2/index.php?SECURE=123
7. OMI-HTAP SO_2 emission dataset is available at https://avdc.gsfc.nasa.gov/pub/data/project/OMI_HTAP_emis/

Appendix A

A1 Meteorological Boundary and Initial Conditions

To be consistent with IC&BC for chemical species and aerosols, we developed a procedure to build meteorological IC&BC from MERRA-2 reanalysis for all required by WRF-Chem meteorological parameters. In particular, the following 3D parameters were processed: pressure (Pa), geopotential height (m), temperature (K), meridional and zonal wind components ($\mathrm{m/s}$), relative humidity (%); 2D parameters: surface pressure (Pa), sea level pressure (Pa), meridional and zonal wind components at $10\mathrm{m}$ ($\mathrm{m/s}$), temperature at $2\mathrm{m}$ (K), relative humidity at $2\mathrm{m}$ (%), skin temperature (K), ice mask (0/1), terrain height (m), land/sea mask (1/0), soil temperature at 0-10 (cm), 10-40 (cm), 40-100 (cm) and 100-200 (cm); soil moisture at 0-10 (cm), 10-40 (cm), 40-100 (cm) and 100-200 (cm); snow depth (m); snow water equivalent ($\mathrm{kg/m^2}$).

A2 Statistics

We calculated the following statistical parameters to quantify the level of agreement between estimations and observations:

Pearson correlation coefficient (R):

$$R = \frac{\sum_{i=1}^{N}\left(F_i - \bar{F}\right)\left(O_i - \bar{O}\right)}{\sqrt{\sum_{i=1}^{N}\left(F_i - \bar{F}\right)^2 \sum_{i=1}^{N}\left(O_i - \bar{O}\right)^2}}. \tag{A1}$$

Root mean square error ($RMSE$):

$$RMSE = \sqrt{\frac{1}{N}\sum_{i=1}^{N}\left(F_i - O_i\right)^2} \tag{A2}$$

Mean $bias$:

$$bias = \frac{1}{N}\sum_{i=1}^{N}\left(F_i - O_i\right) \tag{A3}$$

where F_i is the estimated value, O_i is the observed value, $\bar{F} = \frac{1}{N}\sum_{i=1}^{N} F_i$ and $\bar{O} = \frac{1}{N}\sum_{i=1}^{N} O_i$ their averages and N is the number of data.

A3 Comparison of AERONET and WRF-Chem volume size distributions

The GOCART dust emission formula (2) calculates dust mass flux into the atmosphere within five dust-bins. In this formula the factor C controls the total dust emission mass flux, and the s_p fractions split this flux into five different dust-bins. We assume that $\sum s_p$=1. To match the observed AERONET AVSD we changed the default s_p={0.1, 0.25, 0.25, 0.25, 0.25} to {0.15, 0.1, 0.25, 0.4, 0.1}. It means that 15% of the total dust mass flux is coming as clay and 85% as silt.

In the original formulation the fractions s_p are not normalized and $\sum s_p$=1.1. It is not essential, as the total flux is multiplied by the factor C that is tuned to fit the observed AOD. So we can normalize the original s_p fractions by dividing them to 1.1 and multiplying factor C to 1.1. It will not change any results in eq. (2) but gives the s_p set of {0.09, 0.2275, 0.2275, 0.2275, 0.2275} that is normalized to 1 consistently with our approach. Figure A1 compares the AVSDs calculated with the updated and default s_p fractions for Summer (JJA) of 2015.

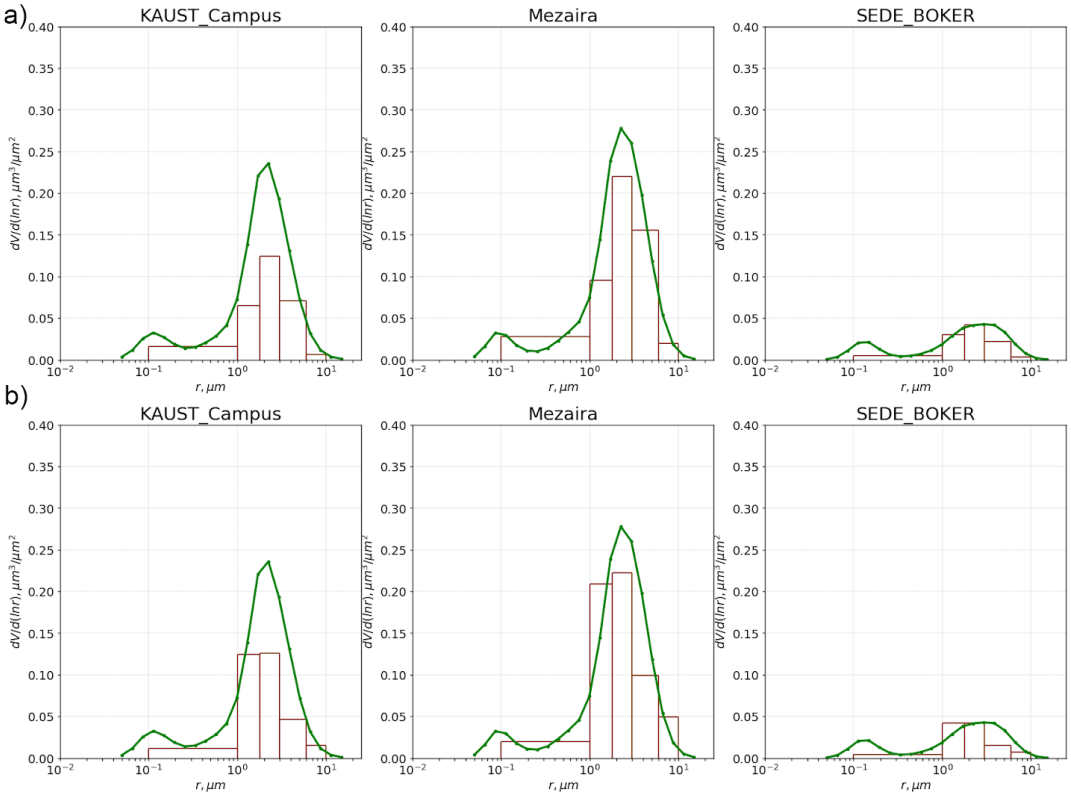

Figure A1. Volume size distributions at *KAUST Campus*, *Mezaira* and *Sede Boker* AERONET sites averaged for JJA of 2015 from WRF-Chem (bars) and from AERONET (solid line): a) updated s_p={0.15, 0.1, 0.25, 0.4, 0.1}, b) default s_p={0.1, 0.25, 0.25, 0.25, 0.25} fractions.

Author contributions. A. Ukhov wrote the manuscript and took part in planning and performing the calculations. S. Mostamandi performed the calculations, constructed meteorological IC&BC based on MERRA-2 reanalysis, prepared MAIAC AOD fields, wrote the section on meteorological conditions, and took part in the discussions. G. Stenchikov planned the calculations, led the discussion, and reviewed and improved the manuscript. I. Shevchenko maintained the *KAUST Campus* AERONET station. Y. Alshehri collected, filtered, and validated PM observational data and wrote the section on the PM measurement procedures. J. Flemming and A. Dasilva participated in the discussion, helped to formulate the research program, and reviewed the manuscript.

Competing interests. The authors declare that they have no conflict of interest.

Acknowledgements. In this work we used AERONET data from the *KAUST Campus* site that was established and maintained by our group with the help of the NASA Goddard Space Flight Center AERONET team. We thank Brent Holben and Alexander Smirnov for the monitoring and regular calibrations of our instruments. We also used data from the *Sede Boker* and *Mezaira* sites and would like to thank their principal investigators Arnon Karnieli and Brent Holben.

We would like to thank Dr. Fei Liu for providing the OMI-HTAP dataset.

The research reported in this publication was supported by funding from King Abdullah University of Science and Technology (KAUST). For computer time, this research used the resources of the Supercomputing Laboratory at KAUST. The authors would like to thank the Saudi Authority for Industrial Cities and Technology Zones (MODON) for sharing their air quality observational data.

We are thankful to Linda and Mark Everett for proofreading this manuscript.

References

Adebiyi, A. A. and Kok, J. F.: Climate models miss most of the coarse dust in the atmosphere, Science Advances, 6, eaaz9507, 2020.

Al-Jahdali, M. and Bisher, A. B.: Sulfur dioxide (SO2) accumulation in soil and plant's leaves around an oil refinery: A case study from Saudi Arabia, American journal of environmental sciences, 4, 84–88, 2008.

Al-Taani, A. A., Nazzal, Y., Howari, F. M., and Yousef, A.: Long-term trends in ambient fine particulate matter from 1980 to 2016 in United Arab Emirates, Environmental monitoring and assessment, 191, 143, 2019.

Alghamdi, M. A., Almazroui, M., Shamy, M., Redal, M. A., Alkhalaf, A. K., Hussein, M. A., and Khoder, M. I.: Characterization and elemental composition of atmospheric aerosol loads during springtime dust storm in western Saudi Arabia, Aerosol Air Qual. Res, 15, 440–453, 2015.

Alharbi, B., Shareef, M. M., and Husain, T.: Study of chemical characteristics of particulate matter concentrations in Riyadh, Saudi Arabia, Atmospheric Pollution Research, 6, 88–98, 2015.

Anderson, J. R.: A land use and land cover classification system for use with remote sensor data, vol. 964, US Government Printing Office, 1976.

Anisimov, A., Tao, W., Stenchikov, G., Kalenderski, S., Prakash, P. J., Yang, Z.-L., and Shi, M.: Quantifying local-scale dust emission from the Arabian Red Sea coastal plain, Atmos. Chem. Phys, 17, 993–1015, 2017.

Anisimov, A., Axisa, D., Kucera, P. A., Mostamandi, S., and Stenchikov, G.: Observations and Cloud-Resolving Modeling of Haboob Dust Storms Over the Arabian Peninsula, Journal of Geophysical Research: Atmospheres, 123, 12–147, 2018.

Archer-Nicholls, S., Lowe, D., Darbyshire, E., Morgan, W., Bela, M., Pereira, G., Trembath, J., Kaiser, J., Longo, K., Freitas, S., et al.: Characterising Brazilian biomass burning emissions using WRF-Chem with MOSAIC sectional aerosol, Geoscientific Model Development, 8, 549–577, 2015.

Banks, J. R., Brindley, H. E., Stenchikov, G., and Schepanski, K.: Satellite retrievals of dust aerosol over the Red Sea and the Persian Gulf (2005–2015), Atmospheric Chemistry and Physics, 17, 3987–4003, 2017.

Benedetti, A., Morcrette, J.-J., Boucher, O., Dethof, A., Engelen, R., Fisher, M., Flentje, H., Huneeus, N., Jones, L., Kaiser, J., et al.: Aerosol analysis and forecast in the European centre for medium-range weather forecasts integrated forecast system: 2. Data assimilation, Journal of Geophysical Research: Atmospheres, 114, 2009.

Buchard, V., da Silva, A., Randles, C., Colarco, P., Ferrare, R., Hair, J., Hostetler, C., Tackett, J., and Winker, D.: Evaluation of the surface PM2. 5 in Version 1 of the NASA MERRA Aerosol Reanalysis over the United States, Atmospheric Environment, 125, 100–111, 2016.

Buchard, V., Randles, C., Da Silva, A., Darmenov, A., Colarco, P., Govindaraju, R., Ferrare, R., Hair, J., Beyersdorf, A., Ziemba, L., et al.: The MERRA-2 aerosol reanalysis, 1980 onward. Part II: Evaluation and case studies, Journal of Climate, 30, 6851–6872, 2017.

Cahill, B., Toumi, R., Stenchikov, G., Osipov, S., and Brindley, H.: Evaluation of thermal and dynamic impacts of summer dust aerosols on the Red Sea, Journal of Geophysical Research: Oceans, 122, 1325–1346, 2017.

Cesnulyte, V., Lindfors, A., Pitkänen, M., Lehtinen, K., Morcrette, J.-J., and Arola, A.: Comparing ECMWF AOD with AERONET observations at visible and UV wavelengths, Atmospheric Chemistry and Physics, 14, 593–608, 2014.

Chin, M., Ginoux, P., Kinne, S., Torres, O., Holben, B. N., Duncan, B. N., Martin, R. V., Logan, J. A., Higurashi, A., and Nakajima, T.: Tropospheric aerosol optical thickness from the GOCART model and comparisons with satellite and Sun photometer measurements, Journal of the atmospheric sciences, 59, 461–483, 2002.

Chin, M., Diehl, T., Tan, Q., Prospero, J. M., Kahn, R. A., Remer, L. A., Yu, H., Sayer, A. M., Bian, H., Geogdzhayev, I. V., Holben, B. N., Howell, S. G., Huebert, B. J., Hsu, N. C., Kim, D., Kucsera, T. L., Levy, R. C., Mishchenko, M. I., Pan, X., Quinn, P. K., Schuster, G. L., Streets, D. G., Strode, S. A., Torres, O., and Zhao, X.-P.: Multi-decadal aerosol variations from 1980 to 2009: a perspective from observations and a global model, Atmospheric Chemistry and Physics, 14, 3657–3690, https://doi.org/10.5194/acp-14-3657-2014, https://www.atmos-chem-phys.net/14/3657/2014/, 2014.

Chuang, M.-T., Zhang, Y., and Kang, D.: Application of WRF/Chem-MADRID for real-time air quality forecasting over the Southeastern United States, Atmospheric Environment, 45, 6241–6250, 2011.

Climate.com: Climate of Middle East, Climate.com, http://climateof.com/middleeast/index.asp, 2018.

Cuevas, E., Camino, C., Benedetti, A., Basart, S., Terradellas, E., Baldasano, J., Morcrette, J.-J., Marticorena, B., Goloub, P., Mortier, A., et al.: The MACC-II 2007-2008 reanalysis: atmospheric dust evaluation and characterization over Northern Africa and Middle East., Atmospheric Chemistry & Physics Discussions, 14, 2014.

Damian, V., Sandu, A., Damian, M., Potra, F., and Carmichael, G. R.: The kinetic preprocessor KPP-a software environment for solving chemical kinetics, Computers & Chemical Engineering, 26, 1567–1579, 2002.

Dubovik, O. and King, M. D.: A flexible inversion algorithm for retrieval of aerosol optical properties from Sun and sky radiance measurements, Journal of Geophysical Research: Atmospheres, 105, 20 673–20 696, 2000.

Engelbrecht, J. P., Stenchikov, G., Prakash, P. J., Lersch, T., Anisimov, A., and Shevchenko, I.: Physical and chemical properties of deposited airborne particulates over the Arabian Red Sea coastal plain, Atmospheric Chemistry and Physics, 17, 11 467–11 490, 2017.

EUEA: Air Quality Standards, European Environment Agency, http://ec.europa.eu/environment/air/quality/standards.htm, 2008.

Farahat, A.: Air pollution in the Arabian Peninsula (Saudi Arabia, the United Arab Emirates, Kuwait, Qatar, Bahrain, and Oman): causes, effects, and aerosol categorization, Arabian Journal of Geosciences, 9, 196, 2016.

Fioletov, V. E., McLinden, C. A., Krotkov, N., Li, C., Joiner, J., Theys, N., Carn, S., and Moran, M. D.: A global catalogue of large SO 2 sources and emissions derived from the Ozone Monitoring Instrument., Atmospheric Chemistry & Physics, 16, 2016.

Flemming, J., Huijnen, V., Arteta, J., Bechtold, P., Beljaars, A., Blechschmidt, A.-M., Diamantakis, M., Engelen, R., Gaudel, A., Inness, A., et al.: Tropospheric chemistry in the Integrated Forecasting System of ECMWF., Geoscientific model development, 8, 2015.

Forkel, R., Werhahn, J., Hansen, A. B., McKeen, S., Peckham, S., Grell, G., and Suppan, P.: Effect of aerosol-radiation feedback on regional air quality–A case study with WRF/Chem, Atmospheric environment, 53, 202–211, 2012.

Furman, H. K. H.: Dust storms in the Middle East: sources of origin and their temporal characteristics, Indoor and Built Environment, 12, 419–426, 2003.

Ginoux, P., Chin, M., Tegen, I., Prospero, J. M., Holben, B., Dubovik, O., and Lin, S.-J.: Sources and distributions of dust aerosols simulated with the GOCART model, Journal of Geophysical Research: Atmospheres, 106, 20 255–20 273, 2001.

Gong, S.: A parameterization of sea-salt aerosol source function for sub-and super-micron particles, Global biogeochemical cycles, 17, 2003.

Goudie, A. S. and Middleton, N. J.: Desert dust in the global system, Springer Science & Business Media, 2006.

Granier, C., Bessagnet, B., Bond, T., D'Angiola, A., van Der Gon, H. D., Frost, G. J., Heil, A., Kaiser, J. W., Kinne, S., Klimont, Z., et al.: Evolution of anthropogenic and biomass burning emissions of air pollutants at global and regional scales during the 1980–2010 period, Climatic Change, 109, 163, 2011.

Grell, G. A., Peckham, S. E., Schmitz, R., McKeen, S. A., Frost, G., Skamarock, W. C., and Eder, B.: Fully coupled "online" chemistry within the WRF model, Atmospheric Environment, 39, 6957–6975, 2005.

Hamidi, M., Kavianpour, M. R., and Shao, Y.: Synoptic analysis of dust storms in the Middle East, Asia-Pacific Journal of Atmospheric Sciences, 49, 279–286, 2013.

Heidinger, A. K., Foster, M. J., Walther, A., and Zhao, X.: The pathfinder atmospheres–extended AVHRR climate dataset, Bulletin of the American Meteorological Society, 95, 909–922, 2014.

Holben, B. N., Eck, T. F., Slutsker, I., Tanre, D., Buis, J., Setzer, A., Vermote, E., Reagan, J., Kaufman, Y., Nakajima, T., et al.: AERONET—A federated instrument network and data archive for aerosol characterization, Remote sensing of environment, 66, 1–16, 1998.

Inness, A., Blechschmidt, A.-M., Bouarar, I., Chabrillat, S., Crepulja, M., Engelen, R., Eskes, H., Flemming, J., Gaudel, A., Hendrick, F., et al.: Data assimilation of satellite-retrieved ozone, carbon monoxide and nitrogen dioxide with ECMWF's Composition-IFS, Atmospheric chemistry and physics, 15, 5275–5303, 2015.

Inness, A., Ades, M., Agusti-Panareda, A., Barré, J., Benedictow, A., Blechschmidt, A.-M., Dominguez, J., Engelen, R., Eskes, H., Flemming, J., et al.: The CAMS reanalysis of atmospheric composition, Atmospheric Chemistry and Physics, 19, 3515–3556, 2019.

Janssens-Maenhout, G., Pagliari, V., Guizzardi, D., and Muntean, M.: Global emission inventories in the Emission Database for Global Atmospheric Research (EDGAR)–Manual (I), Gridding: EDGAR emissions distribution on global gridmaps, Publications Office of the European Union, Luxembourg, 2013.

Janssens-Maenhout, G., Crippa, M., Guizzardi, D., Dentener, F., Muntean, M., Pouliot, G., Keating, T., Zhang, Q., Kurokawa, J., Wankmüller, R., et al.: HTAP_v2: a mosaic of regional and global emission gridmaps for 2008 and 2010 to study hemispheric transport of air pollution., Atmospheric Chemistry & Physics Discussions, 15, 2015.

Jish Prakash, P., Stenchikov, G. L., Kalenderski, S., Osipov, S., and Bangalath, H. K.: The impact of dust storms on the Arabian Peninsula and the Red Sea, Atmospheric Chemistry and Physics, 2015.

Jish Prakash, P., Stenchikov, G., Tao, W., Yapici, T., Warsama, B., and Engelbrecht, J. P.: Arabian Red Sea coastal soils as potential mineral dust sources, Atmospheric Chemistry and Physics, 16, 11 991–12 004, 2016.

Kahn, R. A., Gaitley, B. J., Martonchik, J. V., Diner, D. J., Crean, K. A., and Holben, B.: Multiangle Imaging Spectroradiometer (MISR) global aerosol optical depth validation based on 2 years of coincident Aerosol Robotic Network (AERONET) observations, Journal of Geophysical Research: Atmospheres, 110, 2005.

Kalenderski, S. and Stenchikov, G.: High-resolution regional modeling of summertime transport and impact of African dust over the Red Sea and Arabian Peninsula, Journal of Geophysical Research: Atmospheres, 121, 6435–6458, 2016.

Kalenderski, S., Stenchikov, G. L., and Zhao, C.: Modeling a typical winter-time dust event over the Arabian Peninsula and the Red Sea, Atmospheric Chemistry and Physics, 2013.

Karagulian, F., Belis, C. A., Dora, C. F. C., Prüss-Ustün, A. M., Bonjour, S., Adair-Rohani, H., and Amann, M.: Contributions to cities' ambient particulate matter (PM): A systematic review of local source contributions at global level, Atmospheric environment, 120, 475–483, 2015.

Kaufman, Y. J., Tanré, D., Remer, L. A., Vermote, E., Chu, A., and Holben, B.: Operational remote sensing of tropospheric aerosol over land from EOS moderate resolution imaging spectroradiometer, Journal of Geophysical Research: Atmospheres, 102, 17 051–17 067, 1997.

Khan, B., Stenchikov, G., Weinzierl, B., Kalenderski, S., and Osipov, S.: Dust plume formation in the free troposphere and aerosol size distribution during the Saharan Mineral Dust Experiment in North Africa, Tellus B: Chemical and Physical Meteorology, 67, 27 170, 2015.

Khodeir, M., Shamy, M., Alghamdi, M., Zhong, M., Sun, H., Costa, M., Chen, L.-C., and Maciejczyk, P.: Source apportionment and elemental composition of PM2. 5 and PM10 in Jeddah City, Saudi Arabia, Atmospheric pollution research, 3, 331–340, 2012.

Kim, S.-W., Heckel, A., McKeen, S., Frost, G., Hsie, E.-Y., Trainer, M., Richter, A., Burrows, J., Peckham, S., and Grell, G.: Satellite-observed US power plant NOx emission reductions and their impact on air quality, Geophysical Research Letters, 33, 2006.

Klimont, Z., Smith, S. J., and Cofala, J.: The last decade of global anthropogenic sulfur dioxide: 2000–2011 emissions, Environmental Research Letters, 8, 014 003, 2013.

Klingmüller, K., Pozzer, A., Metzger, S., Stenchikov, G. L., and Lelieveld, J.: Aerosol optical depth trend over the Middle East, Atmospheric Chemistry and Physics, 16, 5063–5073, 2016.

Kok, J. F.: Does the size distribution of mineral dust aerosols depend on the wind speed at emission?, Atmospheric Chemistry and Physics, 11, 10 149–10 156, 2011.

Lelieveld, J., Evans, J. S., Fnais, M., Giannadaki, D., and Pozzer, A.: The contribution of outdoor air pollution sources to premature mortality on a global scale, Nature, 525, 367, 2015.

Levelt, P. F., van den Oord, G. H., Dobber, M. R., Malkki, A., Visser, H., de Vries, J., Stammes, P., Lundell, J. O., and Saari, H.: The ozone monitoring instrument, IEEE Transactions on geoscience and remote sensing, 44, 1093–1101, 2006.

Levy, R., Hsu, C., et al.: MODIS Atmosphere L2 Aerosol Product. NASA MODIS Adaptive Processing System, Goddard Space Flight Center, USA, 2015.

Li, C., Joiner, J., Krotkov, N. A., and Bhartia, P. K.: A fast and sensitive new satellite SO2 retrieval algorithm based on principal component analysis: Application to the ozone monitoring instrument, Geophysical Research Letters, 40, 6314–6318, 2013.

Lihavainen, H., Alghamdi, M., Hyvärinen, A.-P., Hussein, T., Aaltonen, V., Abdelmaksoud, A., Al-Jeelani, H., Almazroui, M., Almehmadi, F., Al Zawad, F., et al.: Aerosols physical properties at Hada Al Sham, western Saudi Arabia, Atmospheric Environment, 135, 109–117, 2016.

Liu, F., Choi, S., Li, C., Fioletov, V. E., McLinden, C. A., Joiner, J., Krotkov, N. A., Bian, H., Janssens-Maenhout, G., Darmenov, A. S., et al.: A new global anthropogenic SO 2 emission inventory for the last decade: a mosaic of satellite-derived and bottom-up emissions, Atmospheric Chemistry and Physics, 18, 16 571–16 586, 2018.

Lyapustin, A., Wang, Y., Korkin, S., and Huang, D.: MODIS Collection 6 MAIAC algorithm., Atmospheric Measurement Techniques, 11, 2018.

Madronich, S.: Photodissociation in the atmosphere: 1. Actinic flux and the effects of ground reflections and clouds, Journal of Geophysical Research: Atmospheres, 92, 9740–9752, 1987.

Marticorena, B. and Bergametti, G.: Modeling the atmospheric dust cycle: 1. Design of a soil-derived dust emission scheme, Journal of Geophysical Research: Atmospheres, 100, 16 415–16 430, 1995.

Martin, R. L. and Kok, J. F.: Wind-invariant saltation heights imply linear scaling of aeolian saltation flux with shear stress, Science advances, 3, e1602 569, 2017.

McLinden, C. A., Fioletov, V., Shephard, M. W., Krotkov, N., Li, C., Martin, R. V., Moran, M. D., and Joiner, J.: Space-based detection of missing sulfur dioxide sources of global air pollution, Nature Geoscience, 9, 496–500, 2016.

Middleton, N.: A geography of dust storms in South-west Asia, Journal of Climatology, 6, 183–196, 1986.

Miguez-Macho, G., Stenchikov, G. L., and Robock, A.: Spectral nudging to eliminate the effects of domain position and geometry in regional climate model simulations, Journal of Geophysical Research: Atmospheres, 109, 2004.

Mohalfi, S., Bedi, H., Krishnamurti, T., and Cocke, S. D.: Impact of shortwave radiative effects of dust aerosols on the summer season heat low over Saudi Arabia, Monthly weather review, 126, 3153–3168, 1998.

Morcrette, J.-J., Boucher, O., Jones, L., Salmond, D., Bechtold, P., Beljaars, A., Benedetti, A., Bonet, A., Kaiser, J., Razinger, M., et al.: Aerosol analysis and forecast in the European Centre for medium-range weather forecasts integrated forecast system: Forward modeling, Journal of Geophysical Research: Atmospheres, 114, 2009.

Munir, S., Habeebullah, T. M., Seroji, A. R., Morsy, E. A., Mohammed, A. M., Saud, W. A., Abdou, A. E., and Awad, A. H.: Modeling particulate matter concentrations in Makkah, applying a statistical modeling approach, Aerosol Air Qual. Res, 13, 901–910, 2013.

Nabat, P., Solmon, F., Mallet, M., Kok, J., and Somot, S.: Dust emission size distribution impact on aerosol budget and radiative forcing over the Mediterranean region: a regional climate model approach., Atmospheric Chemistry & Physics Discussions, 12, 2012.

Notaro, M., Alkolibi, F., Fadda, E., and Bakhrjy, F.: Trajectory analysis of Saudi Arabian dust storms, Journal of Geophysical Research: Atmospheres, 118, 6028–6043, 2013.

Notaro, M., Yu, Y., and Kalashnikova, O. V.: Regime shift in Arabian dust activity, triggered by persistent Fertile Crescent drought, Journal of Geophysical Research: Atmospheres, 120, 2015.

Osipov, S. and Stenchikov, G.: Simulating the regional impact of dust on the Middle East climate and the Red Sea, Journal of Geophysical Research: Oceans, 123, 1032–1047, 2018.

Osipov, S., Stenchikov, G., Brindley, H., and Banks, J.: Diurnal cycle of the dust instantaneous direct radiative forcing over the Arabian Peninsula, Atmospheric Chemistry and Physics, 15, 9537–9553, 2015.

Parajuli, S. P., Stenchikov, G. L., Ukhov, A., and Kim, H.: Dust emission modeling using a new high-resolution dust source function in WRF-Chem with implications for air quality, Journal of Geophysical Research: Atmospheres, 2019.

PME: Ambient Air Quality Standard, The Presidency of Meteorology and Environment, 2012.

Prospero, J. M., Ginoux, P., Torres, O., Nicholson, S. E., and Gill, T. E.: Environmental characterization of global sources of atmospheric soil dust identified with the Nimbus 7 Total Ozone Mapping Spectrometer (TOMS) absorbing aerosol product, Reviews of geophysics, 40, 2–1, 2002.

Provençal, S., Buchard, V., da Silva, A. M., Leduc, R., and Barrette, N.: Evaluation of PM surface concentrations simulated by Version 1 of NASA's MERRA Aerosol Reanalysis over Europe, Atmospheric pollution research, 8, 374–382, 2017.

Randles, C., da Silva, A. M., Buchard, V., Colarco, P., Darmenov, A., Govindaraju, R., Smirnov, A., Holben, B., Ferrare, R., Hair, J., et al.: The MERRA-2 aerosol reanalysis, 1980 onward. Part I: System description and data assimilation evaluation, Journal of climate, 30, 6823–6850, 2017.

Reid, J. S., Piketh, S. J., Walker, A. L., Burger, R. P., Ross, K. E., Westphal, D. L., Bruintjes, R. T., Holben, B. N., Hsu, C., Jensen, T. L., et al.: An overview of UAE2 flight operations: Observations of summertime atmospheric thermodynamic and aerosol profiles of the southern Arabian Gulf, Journal of Geophysical Research: Atmospheres, 113, 2008.

Rienecker, M. M., Suarez, M., Todling, R., Bacmeister, J., Takacs, L., Liu, H., Gu, W., Sienkiewicz, M., Koster, R., Gelaro, R., et al.: The GEOS-5 Data Assimilation System: Documentation of Versions 5.0. 1, 5.1. 0, and 5.2. 0, Tech. rep., NASA Goddard Space Flight Center, Greenbelt, Maryland, 2008.

Ritter, M., Müller, M. D., Tsai, M.-Y., and Parlow, E.: Air pollution modeling over very complex terrain: an evaluation of WRF-Chem over Switzerland for two 1-year periods, Atmospheric research, 132, 209–222, 2013.

Shao, Y.: A model for mineral dust emission, Journal of Geophysical Research: Atmospheres, 106, 20 239–20 254, 2001.

Shao, Y.: Physics and modelling of wind erosion, vol. 37, Springer Science & Business Media, 2008.

Shi, Y., Zhang, J., Reid, J., Holben, B., Hyer, E., and Curtis, C.: An analysis of the collection 5 MODIS over-ocean aerosol optical depth product for its implication in aerosol assimilation, Atmospheric Chemistry and Physics, 11, 557–565, 2011.

Skamarock, W. C., Klemp, J. B., Dudhia, J., Gill, D. O., Barker, D. M., Wang, W., and Powers, J. G.: A description of the advanced research WRF version 2, Tech. rep., National Center For Atmospheric Research Boulder Co Mesoscale and Microscale Meteorology Div, 2005.

Stockwell, W. R., Kirchner, F., Kuhn, M., and Seefeld, S.: A new mechanism for regional atmospheric chemistry modeling, Journal of Geophysical Research: Atmospheres, 102, 25 847–25 879, 1997.

Ukhov, A. and Stenchikov, G.: Merra2BC. Interpolation utility for boundary and initial conditions used in WRF-Chem, https://doi.org/10.5281/zenodo.3695911, 2020.

Ukhov, A., Ahmadov, R., Grell, G., and Stenchikov, G.: Improving dust simulations in WRF-Chem model v4.1.3 coupled with GOCART aerosol module, Geoscientific Model Development Discussions, 2020, 1–30, https://doi.org/10.5194/gmd-2020-92, https://www.geosci-model-dev-discuss.net/gmd-2020-92/, 2020a.

Ukhov, A., Mostamandi, S., Krotkov, N., Flemming, J., da Silva, A., Li, C., Fioletov, V., McLinden, C., Anisimov, A., Alshehri, Y., et al.: Study of SO2 pollution in the Middle East using MERRA-2, CAMS data assimilation products, and high-resolution WRF-Chem simulations, Journal of Geophysical Research: Atmospheres, p. e2019JD031993, 2020b.

USEPA: National Ambient Air Quality Standards, USEPA, https://www.epa.gov/criteria-air-pollutants/naaqs-table, 2010.

van Donkelaar, A., Martin, R. V., Li, C., and Burnett, R. T.: Regional Estimates of Chemical Composition of Fine Particulate Matter using a Combined Geoscience-Statistical Method with Information from Satellites, Models, and Monitors, Environmental science & technology, 2019.

Vaughan, M. A., Young, S. A., Winker, D. M., Powell, K. A., Omar, A. H., Liu, Z., Hu, Y., and Hostetler, C. A.: Fully automated analysis of space-based lidar data: An overview of the CALIPSO retrieval algorithms and data products, in: Laser radar techniques for atmospheric sensing, vol. 5575, pp. 16–30, International Society for Optics and Photonics, 2004.

Wang, X., Liang, X.-Z., Jiang, W., Tao, Z., Wang, J. X., Liu, H., Han, Z., Liu, S., Zhang, Y., Grell, G. A., et al.: WRF-Chem simulation of East Asian air quality: Sensitivity to temporal and vertical emissions distributions, Atmospheric Environment, 44, 660–669, 2010.

WHO: Air quality guidelines: global update 2005, WHO, 2006.

WHO: Ambient air quality and health, WHO, http://www.who.int/en/news-room/fact-sheets/detail/ambient-(outdoor)-air-quality-and-health, 2018.

Yarwood, G., Rao, S., Yocke, M., and Whitten, G.: Updates to the carbon bond chemical mechanism: CB05, Final report to the US EPA, RT-0400675, 8, 2005.

Yu, Y., Notaro, M., Liu, Z., Wang, F., Alkolibi, F., Fadda, E., and Bakhrjy, F.: Climatic controls on the interannual to decadal variability in Saudi Arabian dust activity: Toward the development of a seasonal dust prediction model, Journal of Geophysical Research: Atmospheres, 120, 1739–1758, 2015.

Yu, Y., Notaro, M., Kalashnikova, O. V., and Garay, M. J.: Climatology of summer Shamal wind in the Middle East, Journal of Geophysical Research: Atmospheres, 121, 289–305, 2016.

Zender, C. S., Miller, R., and Tegen, I.: Quantifying mineral dust mass budgets: Terminology, constraints, and current estimates, Eos, Transactions American Geophysical Union, 85, 509–512, 2004.